ACS APPLIED MATERIALS & INTERFACES

www.acsami.org

Forum Article

Metal–Organic Framework- and Polyoxometalate-Based Sorbents for the Uptake and Destruction of Chemical Warfare Agents

Tyler G. Grissom, Anna M. Plonka, Conor H. Sharp, Amani M. Ebrahim, Yiyao Tian, Daniel L. Collins-Wildman, Alexey L. Kaledin, Harrison J. Siegal, Diego Troya, Craig L. Hill, Anatoly I. Frenkel, Djamaladdin G. Musaev, Wesley O. Gordon, Christopher J. Karwacki, Mark B. Mitchell, and John R. Morris*

Cite This: *ACS Appl. Mater. Interfaces* 2020, 12, 14641–14661

Read Online

ACCESS | Metrics & More | Article Recommendations

ABSTRACT: The threat of chemical warfare agents (CWAs), assured by their ease of synthesis and effectiveness as a terrorizing weapon, will persist long after the once-tremendous stockpiles in the U.S. and elsewhere are finally destroyed. As such, soldier and civilian protection, battlefield decontamination, and environmental remediation from CWAs remain top national security priorities. New chemical approaches for the fast and complete destruction of CWAs have been an active field of research for many decades, and new technologies have generated immense interest. In particular, our research team and others have shown metal–organic frameworks (MOFs) and polyoxometalates (POMs) to be active for sequestering CWAs and even catalyzing the rapid hydrolysis of agents. In this Forum Article, we highlight recent advancements made in the understanding and evaluation of POMs and Zr-based MOFs as CWA decontamination materials. Specifically, our aim is to bridge the gap between controlled, solution-phase laboratory studies and real-world or battlefield-like conditions by examining agent–material interactions at the gas–solid interface utilizing a multimodal experimental and computational approach. Herein, we report our progress in addressing the following research goals: (1) elucidating molecular-level mechanisms of the adsorption, diffusion, and reaction of CWA and CWA simulants within a series of Zr-based MOFs, such as UiO-66, MOF-808, and NU-1000, and POMs, including $Cs_8Nb_6O_{19}$ and $(Et_2NH_2)_8[(\alpha\text{-}PW_{11}O_{39}Zr(\mu\text{-}OH)(H_2O))_2]\cdot 7H_2O$, (2) probing the effects that common ambient gases, such as CO_2, SO_2, and NO_2, have on the efficacy of the MOF and POM materials for CWA destruction, and (3) using CWA simulant results to develop hypotheses for live agent chemistry. Key hypotheses are then tested with targeted live agent studies. Overall, our collaborative effort has provided insight into the fundamental aspects of agent–material interactions and revealed strategies for new catalyst development.

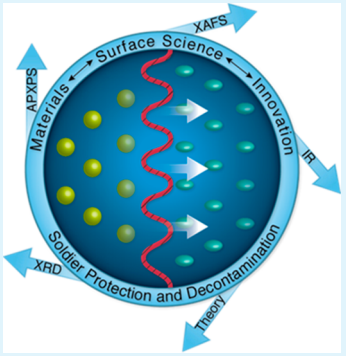

KEYWORDS: *metal–organic frameworks, polyoxometalates, chemical warfare agents*

1. INTRODUCTION

1.1. Historical Perspective. As described throughout in this special issue, chemical warfare agents (CWAs) represent some of the most toxic compounds ever synthesized. The development of advanced agents in the early 20th century ushered in a chemical arms race that peaked in the stockpiling of sarin (GB), soman (GD), sulfur mustard (HD), and VX nerve gas (selected structures shown in Figure 1). The tremendous potency of the nerve agents (such as GB, GD, and VX) arises from irreversible binding to acetylcholinesterase, which leads to a lethal buildup of acetylcholine, a neurotransmitter that performs many functions within the body. While GB and GD are volatile molecules commonly found in the gas phase, VX is a low vapor pressure agent that can persist and accumulate under ambient conditions. Although less toxic, the ease of synthesis and dissemination of HD renders this compound a constant concern. HD is a vesicant agent that leads to blistering and alkylation of biomolecules, especially proteins. The toxicology of CWAs has been and remains an active area of study, with a special emphasis on the development of effective therapeutics and preventative measures for the protection of military and civilian personnel, the latter of which is the primary focus of this Forum Article.

The ever-changing threat of chemical hazards requires new capabilities designed to protect (e.g., through air filtration) and decontaminate (e.g., through physical sequestration or chemical neutralization) personnel and the environment. In general, technologies that incorporate chemical reactions to

Special Issue: Nanomaterial Development, Characterization, and Integration Strategies for Chemical Warfare Defense

Received: November 15, 2019
Accepted: January 17, 2020
Published: January 29, 2020

https://dx.doi.org/10.1021/acsami.9b20833
ACS Appl. Mater. Interfaces 2020, 12, 14641–14661

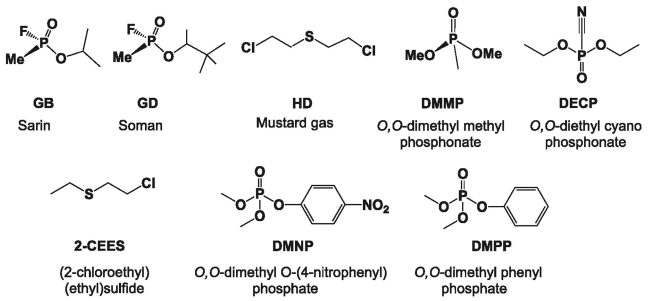

Figure 1. Chemical structures of notable chemical warfare agents and chemical warfare agent simulants. Reprinted from *Chemical Physics*, Vol. *518*, Kaledin, A. L.; Troya, D.; Karwacki, C. J.; Balboa, A.; Gordon, W. O.; Morris, J. R.; Mitchell, M. B.; Frenkel, A. I.; Hill, C. L.; Musaev, D. G. Key mechanistic details of paraoxon decomposition by polyoxometalates: Critical role of para-nitro substitution. **2019**, 30−37 (ref 67). Copyright 2019, with permission from Elsevier.

decompose agents are preferred over methods that rely on simple dilution. For example, solution-based oxidizing agents such as permanganate, hypochlorite salts, liquid and powder bleaching agents, and peroxides have been found to chemically decompose HD and nerve agents (GD, GB, and VX) with a range of efficacies and products that are influenced by the specific chemical environment of the contaminated surface.[1] One drawback of chlorine-based approaches is the effect of corrosion on material surfaces,[2] which has stimulated research into decontaminating chemistries that are more compatible with a wide range of materials employed throughout the military. To reduce some of the corrosive effects of decontaminants, basic chemistries consisting of inorganic hydroxides and amine-based compositions, such as diethylenetriamine, have been employed as effective approaches for decomposing HD, VX, GD, and GB.[3] In addition to solution-based decontamination strategies, a burgeoning area of research focuses on developing methods for air-based agent removal. For example, activated carbons[4] and heterogeneous catalysts[5,6] for agent removal and decontamination show great promise as methods for personnel protection and decontamination.

1.2. Adsorbent-Based Protection. Protection technologies function as the last line of defense for the warfighter to mitigate percutaneous and inhalation exposure to chemical agents that exist as liquid, vapors, gases, and aerosols. The most efficient forms of materials for the capture of chemical agents are solid porous adsorbents, such as activated carbon, for adsorption and retention of low vapor pressure chemicals (G, H series).[7] Modifications to activated carbon were made with the addition of metal salts (Cu, Cr, Zn, Mo) and organics (pyridine, triethylenediamine) for removal of cyanides, such as hydrogen cyanide and cyanogen chloride, and a number of acid-forming chemicals such as phosgene, chlorine, sulfur dioxide, and hydrogen cyanide. Today, activated carbon remains the principal base material used in all U.S. military warfighter protective clothing and filter applications for individual and collective protection applications.[7]

In recent years, a concerted effort has been underway to develop highly efficient porous catalysts that can be easily tailored to a broad spectrum of chemical hazards. A principle aim is to design adsorbent−catalyst materials containing small pores with high adsorption potentials and the capability to rapidly decompose the adsorbed chemical agent under operationally relevant field conditions. In this work, emphasis has been placed on understanding the electronic and geometrical properties of metal- and carbon-based materials, particularly nanostructured clusters within highly ordered crystalline materials, such as metal oxides, metal−organic frameworks, and polyoxometalates. If the present day's research is an indicator of future technologies, there is a strong indication that new capabilities for protection and decontamination of chemical agents will consist of composite materials composed of a variety of structural topologies and active sites that enable rapid adsorption, diffusion, and decomposition of a broad spectrum of chemical threats.

1.3. CWA Decomposition Chemistries. *1.3.1. Hydrolysis-Based Decomposition.* There have been a multitude of papers on catalytic hydrolysis of nerve agents and their simulants, which provide mechanistic and structure−activity information of some value in overcoming the limitations of such processes.[7,8] Both stoichiometric and catalytic nerve-agent hydrolysis reactions have been studied, with the former dominating the earliest studies and the latter dominating more recent studies.[7,8] Nerve-agent hydrolysis catalysts range from transition-metal oxides/hydroxides to coordination compounds, organometallic complexes, and enzymes, and, more recently, to metal−organic frameworks (MOFs) and polyoxometalates (POMs). The latter two classes of materials have been the subject of much research in the last 5 years and are the focus of this Forum Article.

Nerve-agent hydrolysis catalysts, as nearly all catalysts, need to be fast, selective, and stable.[7,9] Speed is evidently important in reducing the risk of a CWA, regardless of the agent formulation or method of deployment. Furthermore, a decontamination catalyst would ideally be fast under ambient conditions. Selectivity is important because CWA degradation products can also be toxic. Preferably, the least toxic product, and that product only, is generated. Stability is important; a catalyst that decomposes quickly under turnover conditions or is badly inhibited by the hydrolysis products is far from ideal. As a catalyst decomposes, it can be rendered inactive, but more worrisome is that a degraded catalyst can continue to function but with lower selectivity, which may generate undesirable products.

Despite the wealth of nerve-agent hydrolysis studies to date, several points are worth noting and not always clear in these studies. First, the great majority of these hydrolysis studies focus on base catalysis and/or cation catalysis (Lewis acid-assisted base or nucleophilic attack at phosphorus). However, other mechanisms could be operable in the same systems at different pH values or under other conditions. Indeed, many slightly to strongly basic hydrolysis systems stop hydrolyzing as neutral pH is approached, but if these same reactions are made quite acidic, hydrolysis can usually begin again. One can write a general rate law for hydrolytic decontamination of organophosphorus (OP) nerve agents such as eq 1 that directly implicates multiple mechanisms and explains the potential importance of pH.[10] Equation 1 has four terms (essentially mechanisms).

$$\text{hydrolysis rate} = (k_{H^+}[H^+] + k + k_{ML_n} + k_{OH^-}[OH^-])[\text{nerve agent}][\text{catalyst}] \quad (1)$$

The first term, $k_{H^+}[H^+]$, designates the acid-catalyzed process (there may be more than one) and is dependent on proton concentration; the third and fourth terms designate processes that are dependent on the metal catalyst, ML_n, and hydroxide,

https://dx.doi.org/10.1021/acsami.9b20833
ACS Appl. Mater. Interfaces 2020, 12, 14641−14661

respectively. There is usually a process that is independent of pH and the catalyst, which proceeds with a rate constant of k. This term, k, and the associated pH-independent mechanism is often ignored, because it is slower and thus of less interest than the terms of usual focus: k_{ML_n} and $k_{OH^-}[OH^-]$. Also, as noted above, the $k_{H^+}[H^+]$ term is frequently overlooked as researchers often omit the assessment of hydrolysis in the presence of strong acid. A related point is that a second cation either inadvertently present in the medium or added to the metal complex catalyst, ML_n, can function as a cocatalyst, and in this case, another term is appropriate in a general rate law like eq 1.

A second critical consideration (especially in the reactions of organophosphonate- and phosphate-containing compounds) that is often ignored in reporting catalytic decontamination (either hydrolysis or oxidation) is that the catalyzed process frequently results in a pH change as the reaction proceeds. In many cases, an equivalent of H^+ or a Lewis acid is generated per equivalent of CWA consumed. This is a minor factor if the decontamination is barely catalytic (stoichiometric or a few turnovers (TONs) of < 5); however, if the TON is 100 or higher, the pH of the medium being decontaminated (unless buffered, which is infrequently the case in realistic field deployment conditions) can become considerably more acidic. This has several consequences. One is that the hydrolysis or oxidation reactions can slow down or completely stop if the base-catalyzed term in the overall rate law ($k_{OH^-}[OH^-]$ in eq 1) is far greater than the other terms; i.e., as $[OH^-]$ gets low, then $k_{OH^-}[OH^-]$ necessarily decreases. In CWA hydrolyses that do not involve a metal complex catalyst (i.e., the k_{ML_n} term in eq 1 is zero), this increase in $[H^+]$ (decrease in $[OH^-]$) during turnover, as neutral pH is approached, will greatly slow the reaction because the k term in the rate law becomes the main rate factor and k is typically small compared to k_{OH^-}.

A third factor that is often ignored in reporting catalytic decontamination is that some hydrolysis reactions can be reversed if the reaction conditions change during the catalytic decontamination reaction itself.[10] For example, base- or base/Lewis acid-catalyzed hydrolysis of VX produces the phosphonic acid/ester (depending on the extent of the hydrolysis) and the thiolate of the side-chain group 2-(diisopropylamino)-ethyl.[11] If there is no buffer and many equivalents of VX are hydrolyzed, the acid generated can reduce the pH sufficiently to where an acid-catalyzed reformation of the P−S bond can take place. In short, VX can be regenerated. One obvious solution to this is to have conditions where the electron-rich and strongly reducing thiolate of the side chain is rapidly oxidized to the corresponding disulfide or other products; then, reformation of VX is avoided. Decontamination systems that simultaneously catalyze the hydrolysis and oxidation of the products might eliminate the concern over the regeneration of the reactants.

A fourth factor to consider in catalytic decontamination is inhibition of the reaction by the products of the reactions themselves. This is a much greater problem for hydrolysis processes than for oxidation ones. Base-dependent and base-plus-Lewis acid-dependent hydrolyses of OP nerve agents result in acid products that strongly hydrogen bond to the nucleophilic hydrolyzing intermediate anions and/or bind to the electrophilic metal center(s). As this review describes, the inhibition results when the hydrolysis products of the nerve agents, either the half-hydrolyzed monoester or the twice-hydrolyzed methyl phosphonic acid (MPA), bind to and inactivate the basic nucleophilic species (e.g., the anionic oxygens in polyniobates that attack the electrophilic OP phosphorus center) by hydrogen bonding. Alternatively, the half-hydrolyzed product or MPA binds strongly to the Zr(IV) centers in Zr-MOFs and Zr-POMs resulting in product inhibition. As described below in this Forum Article, the strongest binding of these products involves a bridging, bidentate, or chelating binding to two adjacent Zr(IV) centers. Strategies that isolate Lewis acidic metal centers may eliminate the tight bidendate binding and product inhibition. Thus, new POMs and MOFs that present different Lewis acidic metal centers in a variety of environments provide a path toward the development of the next generation of decontamination and protection materials.

1.3.2. Oxidation-Based Decomposition. In oxidative decontamination, there are a host of issues to consider, particularly for oxidations based on the most desirable oxidant, the O_2 in ambient air. Chief among these is selectivity, a factor also addressed in the following discussions. This is particularly an issue for sulfur mustard, HD, because the partially oxidized sulfoxide, bis(2-chloroethyl) sulfoxide or HDO, is considerably less toxic than the more oxidized sulfone, bis(2-chloroethyl) sulfone or HDO_2, and the related divinyl sulfone and sulfoxide. The latter are extremely toxic because they can link, like HD itself, a variety of biologically occurring nucleophilic macromolecules. Selectivity is frequently a greater challenge in oxidations than in hydrolyses and some other classes of reactions. This is particularly the case for O_2/air-based oxidations because radical-chain oxidation (autoxidation) is almost always a possibility when O_2 is the terminal oxidant. Unfortunately, autoxidation is rarely selective and can be initiated by traces of most radicals, which themselves can be catalytically produced by some transition metal complexes.

A final point in this overview of catalytic agent decontamination is that reaction conditions matter: many parameters cannot be ignored in studying such processes and optimizing the appropriate catalysts. We recently reported that not only is pH a key in catalytic hydrolysis reactions but also, at constant pH, are (a) the buffer, (b) the buffer concentration, and (c) ionic strength.[70] Also, as discussed later in this Forum Article, the impact on CWA removal of several battlefield contaminants, including the small molecules CO_2, CO, SO_2, and NO_2 and larger species such as hydrocarbons, must be considered. We address, using experimental and complementary computational data, the marked impact of some of these species in catalytic hydrolytic decontamination by MOF and POM systems. Finally, as the subsequent discussion articulates, the relatively safe simulants for CWAs that must be used in most laboratories do differ in properties from the CWAs themselves and the properties of the simulants can impact the catalytic decontamination mechanisms.

1.4. CWA Simulants. In this work, we largely focus on the nerve agents: soman and sarin. These agents, although they do not constitute the majority of CWAs, were selected due to their prominence as immediate threats. However, most studies pertaining to material−nerve agent interactions are performed on simulants that are structurally and chemically similar to the agent of interest but have much lower toxicities. The choice of simulant is challenging because the simulants necessarily provide an incomplete measure of performance against actual agents.[8] The choice of simulant is dependent on the similarity in chemistry, kinetic diameters of the molecules, the electron

https://dx.doi.org/10.1021/acsami.9b20833
ACS Appl. Mater. Interfaces 2020, 12, 14641−14661

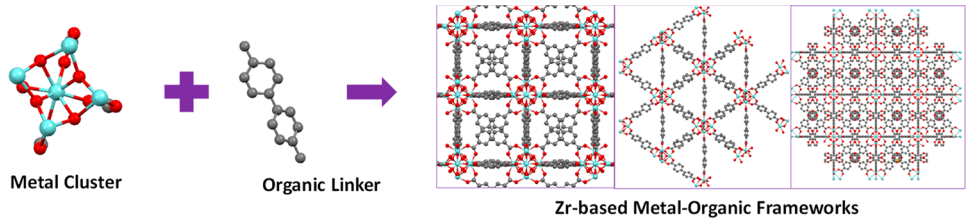

Figure 2. Representative structure of a zirconium-based metal−organic framework.

affinity and electronegativity of the functional groups present, and the strength of interactions with the decontaminant. Agrawal and co-workers examined a multitude of nerve-agent simulants on MOFs that are conducive to sorbent studies on real agents.[12] In their work, they determined the heats of adsorption of over 2900 MOFs for simulants of sarin and soman. They arrived at the conclusion that the most suitable simulant for soman is dimethyl 4-nitrophenylphosphate, DMNP, whereas the most suitable simulant for sarin is dimethyl methyl phosphonate, DMMP, or diethyl chlorophosphate, DCP. The similarity between both the agent and the simulant is in the organophosphorus backbone, which is the essential chemical entity at which the decontamination chemistry occurs. The examination of additional simulants provides insights into the role various functional groups on the live agents may play during decontamination events. CWA simulant studies guide additional experimental work that allow researchers to correlate the behavior of the real agent with a chosen sorbent material and further aid in the development of decomposition methods.

1.5. Metal−Organic Frameworks. MOFs are a class of hybrid organic−inorganic coordination polymers that offer unique avenues for modular synthesis and rational design of engineered materials. They are referred to as coordination networks where both the linker and the metal are connected in a repeating fashion to provide a variety of structures (Figure 2). They are considered a promising class of materials with applications in many interdisciplinary fields, including catalysis, therapeutics,[13] coatings,[14] sensing,[15] separation,[16] gas storage, and filtration.[7] Furthermore, missing organic linkages between metal centers result in defects within the MOF materials, which can be critical to the overall MOF performance.[17,18]

The Computation-Ready, Experimental (CoRE) MOF database has compiled almost 15,000 structures with disorder-free atomic coordinates from the literature.[19] Such a database enables the researcher to choose from the various types of MOFs based on their surface areas, porosities, pore sizes and shapes, thermal and mechanical properties, and chemical stability relevant to the application of interest. Particularly, MOFs have emerged as candidate materials for the adsorption, filtration, and decontamination of toxic industrial chemicals (TICs) and CWAs.[7] The tunable parameters of MOFs described above facilitate the selective removal of acidic, basic, or neutral gases.

The development of the most effective MOF-based technologies for the capture and decontamination of harmful compounds requires a detailed insight into the structural, physical, and chemical properties of the candidate materials. An example in which the knowledge of fundamental chemical properties of an analyte of interest guided material design is the decontamination of the toxic gas ammonia, a basic molecule with a pK_a greater than 30. Utilizing physicochemical information, researchers hypothesized and then demonstrated that the incorporation of Lewis acidic sites, such as Zn_4O clusters found within MOF-177 and MOF-5, leads to the effective removal of ammonia from a gas source.[20] Other research has shown that acid−base interactions between MOFs and gases are the driving force for the separation and filtration of toxic compounds in effluent streams from industrial processes.[21] For example, a well-known and widely used copper-based MOF, HKUST-1, with open Cu^{2+} centers and partial Lewis acidity and basicity is one of the best MOF candidates for the removal of multiple TICs.[17] However, a major drawback of HKUST-1, as with many other MOFs, is its instability upon water exposure.

1.5.1. Zr-Based MOFs. A family of Zr-based MOFs, the UiO (University of Oslo) series,[22] NU-1000,[23,24] and MOF-808, with zirconium nodes, $Zr_6O_4(OH)_4(COO)_{12}$, and different carboxylate ligands (Figure 3) overcome many of the stability

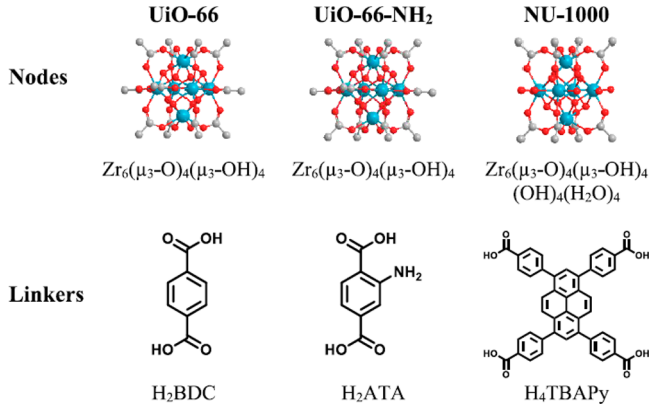

Figure 3. Nodes and linkers of the Zr-based MOFs UiO-66, UiO-66−NH_2, and NU-1000. Atom colors: Zr (blue), O (red), and C (gray). H is omitted for clarity. Reprinted from Wang, H.; Mahle, J. J.; Tovar, T. M.; Peterson, G. W.; Hall, M. G.; DeCoste, J. B.; Buchanan, J. H.; Karwacki, C. J. Solid-Phase Detoxification of Chemical Warfare Agents using Zirconium-Based Metal Organic Frameworks and the Moisture Effects: Analyze via Digestion. *ACS Appl. Mater. Interfaces* **2019**, *11*, 21109−21116 (ref 29). Copyright 2019 American Chemical Society.

issues exhibited by other MOFs and have shown great promise for the capture and decontamination of nerve agents and their simulants.[25] The strong Zr−O bonds afford materials with exceptional thermal and chemical stability, including resistance to the hydrolytic decomposition on exposure to water. The robustness of Zr-MOFs spurred research into the use of these materials for CWA sorption and destruction.[25−29] Liquid-phase hydrolysis studies of DMNP on UiO-66 and UiO-67 indicated that the pore aperture is an important factor in CWA-simulant chemistry. Thus, UiO-67, with a large pore aperture of 11.5 Å, has been observed to reduce the half-life of DMNP by up to 7 orders of magnitude over its smaller analog

https://dx.doi.org/10.1021/acsami.9b20833
ACS Appl. Mater. Interfaces 2020, 12, 14641−14661

UiO-66, which has a pore window of 6 Å.[25] Wang et al. found that the adsorption of DMMP on low-defect density Zr-based MOFs is primarily reversible with physisorption being the dominant process.[30]

Guided by these studies, Ruffley et al. screened functionalized carboxylate ligands using density functional theory (DFT) to better understand how nerve agents can be destroyed and to determine if the energetics of MOF−CWA interactions on UiO-67 derivatives can be tuned to improve reaction efficiency.[26] Their research showed that the amine-functionalized benzene diphenyl carboxylate (BDPC) ligand (at the ortho position) resulted in the strongest binding of DMMP (−73 kJ/mol) within the MOF, whereas the pristine ligand had the weakest interactions with DMMP (−62 kJ/mol). The methylated BDPC ligand offered an intermediate binding energy (−70 kJ/mol). In their studies, they observed that, regardless of the UiO-67 derivative used, the adsorption−desorption process followed first-order kinetics with the complete removal of DMMP at 473 K.[26] This prediction was also supported by their experimental studies, which verified a differential affinity of the UiO-based MOFs toward CWA uptake.

In another study, the adsorption and decontamination of DMMP on Zr-based MOFs with different linkers, UiO-66 (benzene 1,4-dicarboxylate, BDC), UiO-67 (BDPC), MOF-808 (benzene tricarboxylate, BTC), and NU-1000 (tetratopic 1,3,6,8-tetrakis (*p*-benozate)), revealed that the configurational geometry, pore volume, and framework topology also play a role in the MOF−CWA interactions.[27] MOF-808 was the best candidate as a DMMP adsorbent due to the accessibility of DMMP to the pores with almost 1.3% in cell volume expansion after an hour of continuous exposure to DMMP vapors. Fourier analysis revealed that the highest electron density, which correlates to the locations of the molecular DMMP, is found around the Zr_6 clusters.[27] Wang et al. performed a detailed study into the effect of water on the uptake and degradation of soman and the nerve-agent simulant DMNP on UiO-66 and its aminated analog, UiO-66 NH_2.[29] Importantly, their work determined that solid−gas and solid−liquid interactions are different and the amount of water present in the system plays an important role in the decontamination kinetics (Figure 4).

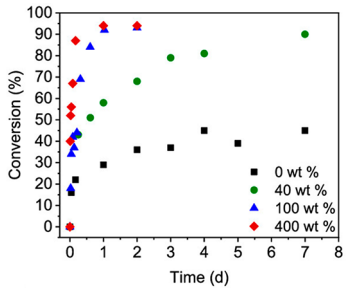

Figure 4. Solid-phase decontamination of the nerve-agent simulant dimethyl-4-nitrophenyl phosphate (DMNP) by UiO-66 with various water loadings. Adapted from Wang, H.; Mahle, J. J.; Tovar, T. M.; Peterson, G. W.; Hall, M. G.; DeCoste, J. B.; Buchanan, J. H.; Karwacki, C. J. Solid-Phase Detoxification of Chemical Warfare Agents using Zirconium-Based Metal Organic Frameworks and the Moisture Effects: Analyze via Digestion. *ACS Appl. Mater. Interfaces* **2019**, *11*, 21109−21116 (ref 29). Copyright 2019 American Chemical Society.

Several studies on Zr-based MOFs have focused on identifying the binding sites for CWAs. The strongest binding sites have been identified as Zr^{4+}, hydroxyl groups, and undercoordinated Zr^{n+} sites.[17,28,30] Modeling, in conjunction with experimental techniques, has confirmed that the most favorable binding sites for sarin are the undercoordinated Lewis acid sites. These Zr^{4+} sites, located at missing-linker defects or at otherwise undercoordinated secondary building units, are critical for agent−MOF chemistry because they are the sites of adsorption, binding, and activated hydrolysis. Favorable agent or simulant binding arises from the fact that undercoordinated metals offer strong Lewis acid sites for organophosphonate interactions or where aqua ligands can bind to form Zr−OH groups that stabilize the P═O bond via hydrogen bonding.[31] Indeed, the phenomenon of binding at the defect site has been computationally shown and supported by experimental studies. In that work, spectroscopic evidence was presented that showed adsorption occurs at multiple binding sites (i.e., at Zr metal sites, undercoordinated metal sites, and μ_3-OH sites) within UiO-66. In another study, the effect of defect density on MOF−soman interactions in UiO-66−NH_2 revealed the complexities in quantifying the defect density and allocation of defect sites. Nonetheless, an increase in the number of defects was hypothesized to improve the hydrolysis efficiency of soman and DMNP within the MOF.[18]

1.6. Polyoxometalates. In addition to examining Zr-based MOFs as decontamination materials for CWAs, we have investigated an alternative class of materials known as polyoxometalates. POMs comprise a group of molecular, highly tunable, metal−oxygen anions that are important in a wide variety of chemical applications including medicine, catalysis, and materials science (Figure 5).[32,33] Similar to

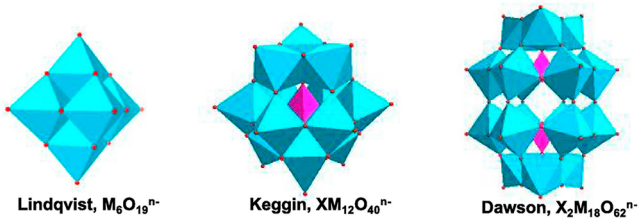

Figure 5. Representations of common classes of polyoxometalates. The blue octahedra are MO_6 units, and the purple tetrahedra are internal XO_4. Reprinted from *Chemical Physics*, Vol. *518*, Kaledin, A. L.; Troya, D.; Karwacki, C. J.; Balboa, A.; Gordon, W. O.; Morris, J. R.; Mitchell, M. B.; Frenkel, A. I.; Hill, C. L.; Musaev, D. G. Key mechanistic details of paraoxon decomposition by polyoxometalates: Critical role of para-nitro substitution. **2019**, 30−37(ref 67). Copyright 2019, with permission from Elsevier.

MOFs, many researchers have successfully utilized the highly modular properties of these compounds for the decontamination of chemical warfare agents. The two classes of chemical warfare agents are generally detoxified via different pathways: hydrolysis for organophosphorus nerve agents and oxidation for sulfide/amine-based blister agents.[17] This results in certain materials being optimized often for one type of agent or the other. For nerve agents, a wide variety of POMs were shown to catalyze hydrolysis including polymolybdates, polyniobates, and polytungstates.[34−38] For these reactions, the electron-rich oxygen centers, as shown via DFT calculations on $Cs_8Nb_6O_{19}$,[36] help the POM to act as a general-base catalyst. Other studies enhanced hydrolysis rates by incorporating

https://dx.doi.org/10.1021/acsami.9b20833
ACS Appl. Mater. Interfaces 2020, 12, 14641−14661

Lewis acidic centers such as zinc and zirconium, similar to those found in MOFs, either as counter cations or as a part of the POM framework.[39−41,70] In these systems, the Lewis acid sites activate the phosphorus−oxygen, or in some cases phosphorus−sulfur, double bond, making the nerve agent more susceptible to nucleophilic attack by water or hydroxide.[42]

On the oxidative side, POMs are well-known to catalyze sulfide oxidations in the presence of hydrogen peroxide.[33] A number of groups have used polymolybdates, polyniobates, and polytungstates in the presence of H_2O_2 to oxidize both sulfur mustard (HD) and its simulant 2-chloroethylethyl sulfide (2-CEES).[34,35,37,40,41] Further, Buru et al. incorporated $H_3PW_{12}O_{40}$ into the pores of the zirconium-based MOF, NU-1000, creating a heterogeneous POM−MOF oxidation catalytic material.[43] In an effort to avoid the use of hydrogen peroxide, Hill and co-workers explored POM-catalyzed oxidation using air-based oxygen to drive the reaction.[44,45] Given the significant degree of overlap between POMs used for catalyzing both sulfide oxidation and organophosphorus hydrolysis, a number of studies have successfully demonstrated activity with a single material for both reactions.[34,35,37,40,41] In this Forum Article, we highlight specific examples, from our joint research effort, of POM-based catalysis that provide greater detail regarding reaction mechanisms and practical considerations toward the development of deployable detoxifying materials.

2. SPOTLIGHT ON MULTIDISCIPLINARY RESEARCH FOR AGENT DESTRUCTION

In the previous sections, we highlighted the promising potential of both MOFs and POMs as next-generation decontamination sorbent and possibly catalytically active materials; however, a major hurdle in their development is understanding how the materials operate under ambient or battlefield conditions, specifically, vapor-phase exposures in both the absence and presence of ambient gases. The aim of this Forum Article is to present our research efforts addressing two major gaps in the field of adsorbent-based CWA decontamination materials: (1) to understand the interfacial chemistry that occurs upon vapor-phase exposure of CWA and CWA simulants on both MOF- and POM-based materials and (2) to elucidate the effects that ambient gases such as H_2O, CO, CO_2, SO_2, and NO_2 as well as possible battlefield contaminants including aliphatic and aromatic hydrocarbons have on the decontamination efficacy of both MOF and POM materials. Our multidisciplinary research team utilizes *in situ* and *in operando*-based experimental techniques combined with high-level computational methods to help bridge the gap between solution-phase laboratory studies and real-world performance. This Forum Article summarizes important advances made by our research team over the past few years.

2.1. Metal−Organic Frameworks. *2.1.1. Diffusion of Organic Compounds through MOFs.* The extent to which CWA molecules access the inner pore environment of MOFs, where potential sorption or reaction sites reside, ultimately limits the efficacy of the material as a catalyst. The advantage that the tremendously high surface areas of MOFs offers can only be realized for systems that exhibit rapid diffusion of CWAs to the active sites and efficient transport of products from those sites. Thus, a detailed, molecular-level understanding of the diffusion mechanism and rates of compounds within MOFs can guide rational design of next-generation MOF-based decontamination materials.

With the goal of evaluating the transport dynamics of CWAs in Zr-based MOFs, our research efforts began by developing a method for monitoring molecular transport under pristine conditions. Our approach, adapted from Kim et al.,[46] utilized in situ infrared (IR) spectroscopy operating under ultrahigh vacuum (UHV) conditions to monitor changes that occur during exposure, diffusion, and desorption of the analytes of interest within porous materials, specifically Zr-based MOFs.[30,46−48] Initial diffusion studies were performed on UiO-66 with a series of linear and aromatic hydrocarbons to validate the method.[47,48] Hydrocarbons were chosen for the initial studies due to their relatively low complexity compared to CWA systems as well as due to their importance in petrochemical, environmental, and military-related fields.

Upon exposure to each of the hydrocarbons of interest, perturbations of the $\nu(\mu_3\text{-O−H})$ mode of UiO-66 (3674 cm^{-1}) provide clear spectroscopic evidence that each analyte was able to access the inner pore environment of UiO-66 (Figure 6). The *m*- and *o*-xylene molecules, which have kinetic

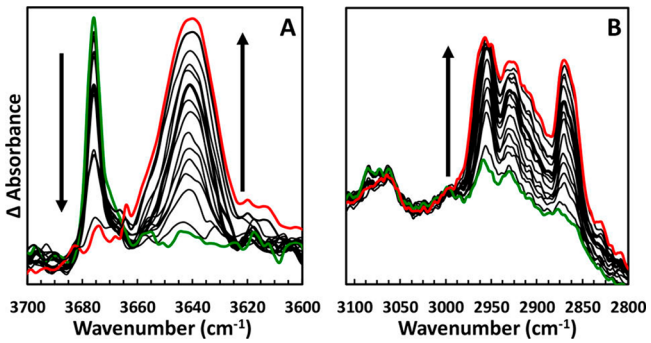

Figure 6. IR spectra *n*-butane adsorption on UiO-66. (A) O−H and (B) and C−H stretching regions. Reprinted from Sharp, C. H.; Abelard, J.; Plonka, A. M.; Guo, W.; Hill, C. L.; Morris, J. R. Alkane−OH Hydrogen Bond Formation and Diffusion Energetics of *n*-Butane within UiO-66. *J. Phys. Chem. C* **2017**, *121*, 8902−8906 (ref 47). Copyright 2017 American Chemical Society.

diameters (6.8 Å)[49] on the same size scale as the pore apertures of UiO-66 (6.5 Å),[47] likely require dihedral rotation of the of the organic linkers for passage to be possible.[50] Isothermal diffusion studies, in which characteristic C−H or C−D vibrational modes associated with the adsorbed analytes of interest were monitored during diffusion and desorption from UiO-66, revealed fully reversible analyte−MOF interactions. Modeling the gas transport with Fick's second law yielded diffusion coefficients for each analyte at several temperatures spanning from 173 to 363 K (Table 1). The calculated diffusion coefficients ranged from 2.58×10^{-11} to 9.24×10^{-9} cm^2 s^{-1} depending on the analyte−temperature pair and increased as the sample temperature increased.[47,48]

The diffusion rates of the analytes were strongly dependent on the kinetic diameter of each compound. *n*-Butane and *n*-pentane, which have kinetic diameters much smaller than the dimensions of the pore aperture of UiO-66, diffused much faster than the bulkier aromatic compounds at a given temperature (Table 1). Similarly, benzene and toluene diffused faster than each of the xylene isomers. Interestingly, the diffusion rates of benzene and toluene are almost identical, which was not expected due to the additional methyl group on

https://dx.doi.org/10.1021/acsami.9b20833
ACS Appl. Mater. Interfaces 2020, 12, 14641−14661

Table 1. Diffusivities and Activation Energies of Diffusion for Select Hydrocarbons in UiO-66[43,44]

compound	diffusivity (233 K) (10^{-10} cm^2 s^{-1})	diffusivity (283 K) (10^{-10} cm^2 s^{-1})	E_{Diff} (kJ/mol)
n-butane	8.75[a]		21.0 ± 1.2
n-pentane	13.8		36.5 ± 2.4
benzene-d_6	1.68	45.4	32.9 ± 1.9
toluene-d_8	1.71	41.7	34.7 ± 1.1
p-xylene-d_{10}		10.2	42.7 ± 2.2
m-xylene-d_{10}		4.18	44.2 ± 2.5
o-xylene-d_{10}		0.47	44.2 ± 2.4

[a]213 K.

toluene that one might hypothesize leads to slightly stronger dispersive interactions during transport.

In all cases, the observed exponential increase in diffusivity with increasing temperature suggested hydrocarbon diffusion through UiO-66 is an activated process. As such, activation energies of diffusion (E_{Diff}), which provide insight into the diffusion-limiting step of transport, were calculated using an Arrhenius-type analysis (Figure 7) and were found to range

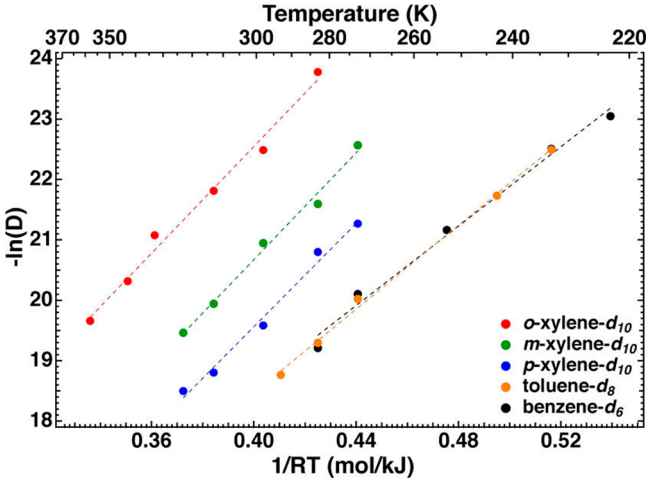

Figure 7. Arrhenius plot for benzene-d_6 (black), toluene-d_8 (orange), *p*-xylene-d_{10} (blue), *m*-xylene-d_{10} (green), and *o*-xylene-d_{10} (red) diffusion through UiO-66 based on a Fickian diffusion model. Reprinted from Grissom, T. G.; Sharp, C. H.; Usov, P. M.; Troya, D.; Morris, A. J.; Morris, J. R. Benzene, Toluene, and Xylene Transport through UiO-66: Diffusion Rates, Energetics, and the Role of Hydrogen Bonding. *J. Phys. Chem. C* **2018**, *122*, 16060−16069 (ref 48). Copyright 2018 American Chemical Society.

from 21 to 45 kJ/mol across the series of selected hydrocarbons (Table 1).[47,48] The Arrhenius fits revealed that, among the aromatic compounds, benzene and toluene have similar activation energies of about 34 kJ mol^{-1}, while the three xylene isomers have much larger but consistent values of 43−44 kJ mol^{-1}. The similarity in E_{Diff} values between benzene and toluene suggests that the diffusion-limiting step is not a result of dispersive interactions between the compound and the MOF. It was determined that, for the bulky aromatic compounds, passage through the 6.5 Å triangular apertures located at the octahedral−tetrahedral pore interface was the rate-limiting process. As a result, the 10 kJ/mol increase in E_{Diff} from benzene and toluene to the xylene isomers was attributed to the added steric hindrance of the molecules, which resulted in greater distortion of the triangular window as the larger xylene isomers passed through the pore apertures.[48]

For the linear-alkane transport, a comparison of the activation energies of diffusion for butane through the hydroxylated versus the dehydroxylated form of UiO-66 revealed the diffusion-limiting step to be breakage of the $-CH_3\cdots\mu_3$-OH hydrogen bond.[47] The small kinetic diameter of the linear alkanes resulted in more efficient passage through the triangular pore apertures relative to the bulkier aromatic compounds. In contrast, no difference in E_{Diff} values was observed for *p*-xylene diffusion through hydroxylated versus dehydroxylated UiO-66, despite differences in the rate of diffusion. Similar activation energies, but varying rates of transport, suggest that the diffusion rate-limiting step for the bulkier molecules is the passage through the triangular apertures and other, relatively low energy dispersive interactions control the overall diffusivity.[48]

Overall, our research efforts into the transport dynamics of compounds through UiO-66 highlight how the topological features within MOFs must be considered together with the characteristics of guest molecules to predict transport rates. Particularly, our results can be extended to better understand the uptake, migration, and binding mechanism associated with CWAs and CWA simulants.

2.1.2. Uptake and Decomposition of DMMP and DMCP within Zr-Based MOFs. A major aim of our research efforts is to understand how nerve agents in the gas phase adsorb, diffuse, and react with Zr-based MOFs. To achieve this, we employ similar in situ infrared spectroscopic methods discussed in the previous section, combined with ambient pressure-based synchrotron powder X-ray diffraction (PXRD) and synchrotron extended X-ray absorption fine-structure (EXAFS) spectroscopy, to monitor the interactions and reactions between the nerve-agent simulants dimethyl methylphosphonate (DMMP) and dimethyl chlorophosphate (DMCP), and a series of Zr-based MOFs.[27,30] While GC-MS, UV−vis, and phosphorus-31 nuclear magnetic resonance (^{31}P NMR) spectroscopy have been traditionally employed to monitor nerve agent and nerve-agent simulant degradation in solution-phase studies,[17] they provide limited information about the chemistry that occurs on the surface of the MOF materials. Furthermore, these techniques are largely unable to examine gas−solid systems and instead are generally limited to materials in solution. The use of in situ FTIR, synchrotron PXRD, EXAFS, and X-ray photoelectron spectroscopy (XPS) overcome these limitations by providing the ability to track molecular-level changes at the surface of the material down to the atomic scale upon gas-phase exposure at varying temperature and chemical environments.

Nerve-agent simulant uptake studies were conducted on five Zr-based MOFs, UiO-66, UiO-66−NH_2, UiO-67, MOF-808, and NU-1000, each of which was composed of the same Zr_6 oxocluster-based inorganic node.[30] Previous computational studies suggest undercoordinated zirconium sites located on the MOF node, either intrinsic to the MOF structure or through the presence of defects, are largely responsible for the catalytic hydrolysis observed in the solution-based studies.[18,28]

Our FTIR results revealed that both DMMP and DMCP physisorbed onto each of the Zr-based MOFs, as evidenced by infrared features consistent with the corresponding condensed-phase simulant (Figures 8 and 9, blue traces).[30] In addition, the simultaneous depletion of the ν(O−H) feature near 3674

https://dx.doi.org/10.1021/acsami.9b20833
ACS Appl. Mater. Interfaces 2020, 12, 14641−14661

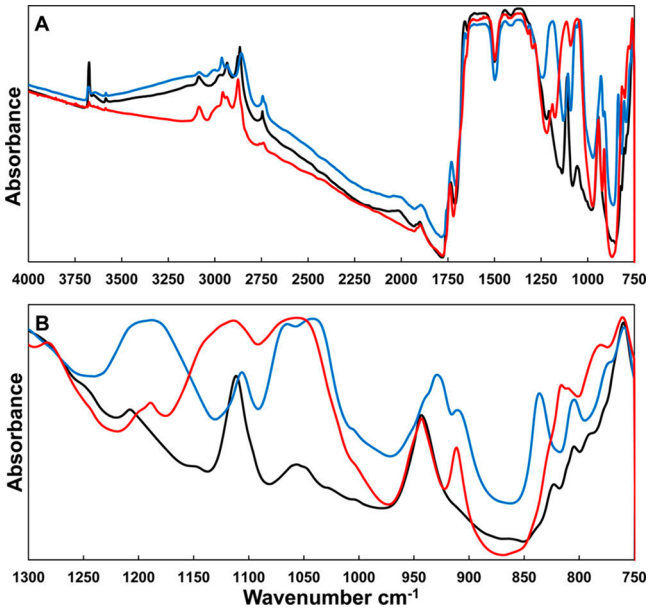

Figure 8. IR spectra of (A) the mid-IR region and (B) the "finger print region of MOF-808 before DMMP exposure (black), after DMMP exposure (blue), and after post-exposure thermal treatment to 600 K (red). Reprinted from Wang, G.; Sharp, C.; Plonka, A. M.; Wang, Q.; Frenkel, A. I.; Guo, W.; Hill, C.; Smith, C.; Kollar, J.; Troya, D., Morris, J. R. Mechanism and Kinetics for Reaction of the Chemical Warfare Agent Simulant, DMMP(g), with Zirconium(IV) MOFs: An Ultrahigh-Vacuum and DFT Study. *J. Phys. Chem. C* **2017**, *121*, 11261−11272 (ref 30). Copyright 2017 American Chemical Society.

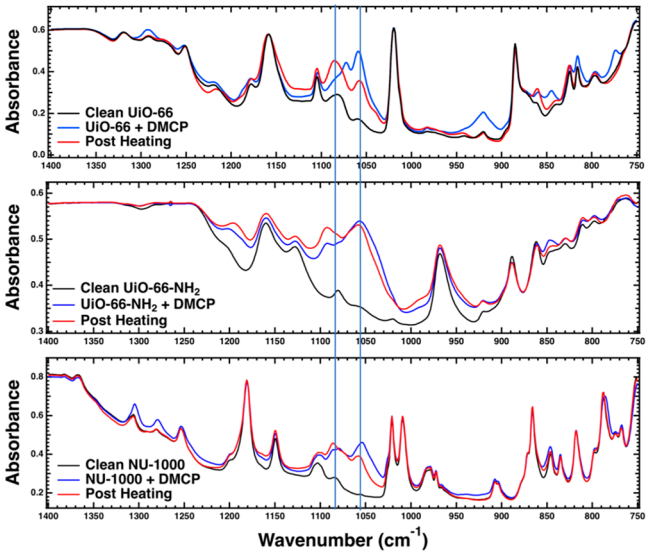

Figure 9. IR summary of the DMCP reaction and irreversible binding on (top) UiO-66, (middle) UiO-66−NH_2, and (bottom) NU-1000: (black) clean, (blue) maximum DMCP coverage, and (red) post-heating. The vertical blue traces guide the eyes to the positions of the ν(P═O) features across the three MOFs.

cm^{-1} associated with the free hydroxyl groups located on the MOFs and the formation of a red-shifted ν(O−H) band indicates both simulants form hydrogen bonds with each of the Zr-based MOFs. However, uptake of DMMP and DMCP onto the smaller-pored Zr-MOFs, UiO-66, and UiO-66−NH_2 resulted in only a limited occupancy of the μ_3-OH groups, whereas significant depletion of the free hydroxyl was observed in the larger-pored MOFs, UiO-67, MOF-808, and NU-1000 (Figure 8A). This suggests the triangular apertures of UiO-66 and UiO-66−NH_2 are too small for DMMP and DMCP to access the pore environments of either MOF, rendering the majority of the potential active sites are inaccessible for nerve-agent destruction, unless missing-linker defects are present.

Several isothermal diffusion experiments similar to those described in the previous section were attempted with the nerve-agent simulants; however, minimal diffusion and desorption were observed even at room temperature. While no experimental diffusion coefficients or energetics could be obtained from these studies, recent computational efforts by Agrawal et al. revealed that diffusion of DMMP through UiO-66 is extremely slow (1.6×10^{-13} cm^2 s^{-1}) and has a relatively high activation energy required to pass through the small triangular pore apertures (56.1 kJ/mol).[51] Upon heating the samples, evidence for desorption of physisorbed DMMP and DMCP was observed, which indicates unreacted simulants resided on the surface of the MOFs. However, the development of prominent IR features between 1080 and 1120 cm^{-1}, consistent with new ν(O−P−O) modes, appeared in both the DMMP and DMCP systems across the entire series of Zr-MOFs examined (Figures 8 and 9, red traces), which suggests DMMP and DMCP react on the surface of each MOF in a similar manner. Further heating up to 600 K accelerated the desorption of physisorbed DMMP and DMCP as well as the growth of the new feature near 1100 cm^{-1}. The persistence of the new ν(O−P−O) features at high temperatures indicates a strongly bound reaction product, which we have determined to be a bidentate-bound phosphate/phosphonate species remaining on the surface of the MOF.

Results from the X-ray-based spectroscopic techniques provide complementary information to the infrared-based studies.[27,30] XPS results from the P 2p region for the post-DMMP and post-DMCP exposed Zr-MOFs confirmed the presence of irreversibly bound phosphorus-containing species remaining on the samples following heating up to 600 K and re-exposure to ambient conditions. Furthermore, shifts in the Zr $3d_{3/2}$ and Zr $3d_{5/2}$ modes indicate a change in the electronic environment of the zirconium species. The observed changes in the electronic environment of the Zr species are consistent with the results gathered from EXAFS studies of the Zr K-edge where the Zr−O and Zr−Zr peaks decreased due to the increased disorder as DMMP molecules directly interact with Zr. The in situ PXRD results revealed that each of the Zr-MOF samples experienced lattice expansion upon exposure to DMMP vapor, consistent with molecules diffusing into the pore environment (Figure 10). While diffusion into the larger-pored MOFs was expected, the expansion of the UiO-66 framework is likely explained by the presence of missing-linker defects, which provide a path for DMMP diffusion into the inner pore environment.

For the DMCP-exposed samples, the examination of the C 1s and Cl 2p regions of the XPS data provided insight into which bonds, P−OCH_3 and/or P−Cl, were broken during the hydrolysis reaction. The C 1s region reveals the growth of a small feature between 286 and 287 eV, consistent with the binding energy reported for the −OCH_3 moiety of DMMP on the metal-oxide systems.[52] These results are consistent with the FTIR results that show the MOF still contained residual −CH_3 species after heating. However, no peaks were observed in the Cl 2p region following DMCP exposure, which reveals two key

https://dx.doi.org/10.1021/acsami.9b20833
ACS Appl. Mater. Interfaces 2020, 12, 14641−14661

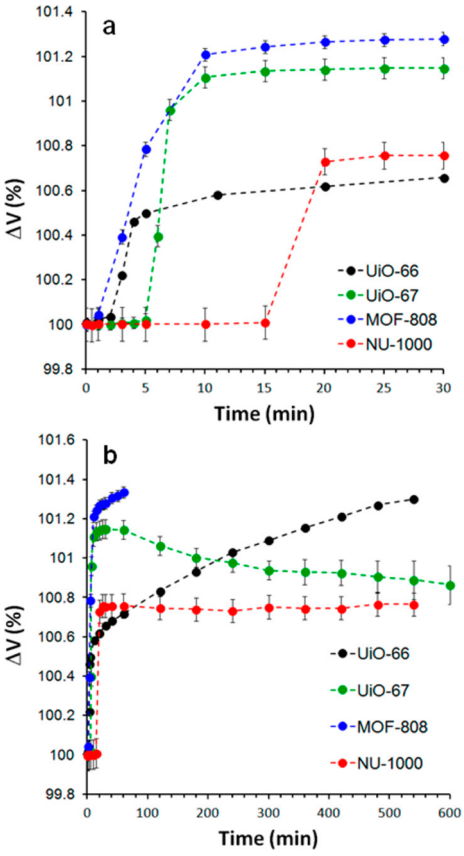

Figure 10. Evolution of UiO-66, UiO-67, MOF-808, and NU-1000 unit cell volumes with the dosing of DMMP: (a) first 30 min of dosing and (b) full experiment. Reprinted from Plonka, A. M.; Wang, Q.; Gordon, W. O.; Balboa, A.; Troya, D.; Guo, W.; Sharp, C. H.; Senanayake, S. D.; Morris, J. R.; Hill, C. L., Frenkel, A. I. *In Situ* Probes of Capture and Decomposition of Chemical Warfare Agent Simulants by Zr-Based Metal Organic Frameworks. *J. Am. Chem. Soc.* **2017**, *139*, 599−602 (ref 27). Copyright 2017 American Chemical Society.

insights to the structure of the DMCP species within the MOF. The first is that no molecularly adsorbed (intact) DMCP remained in the pores of the MOF following heating. Second, the absence of chlorine in the XPS spectrum provides evidence of the chlorine elimination hydrolysis pathway where the bound DMCP reacts on the surface of the MOF and the P−Cl bond is cleaved. Computational studies of sarin on UiO-66 reveal that both HF and isopropyl alcohol can be produced during hydrolysis, but the alcohol elimination pathway is more thermodynamically favorable.[28] Considering that the P−Cl bond is much more labile than the P−F bond, it is not surprising that the Cl elimination pathway was observed for DMCP.

While minimal information regarding catalytic behavior can be elucidated from these studies alone, the presence of the irreversibly bound reaction products indicates that at some point the reaction sites on the MOFs undergo chemical transformation, which may preclude further reactions (catalytic turnover). On-going studies that are examining the gas-phase effluent will help bridge the gap between the solution-phase catalytic studies and those presented here.

Furthermore, the similarities of the final FTIR and XPS spectra across the DMMP- and DMCP-exposed Zr-MOFs indicate a similar irreversibly bound reaction product forms in each of the systems examined in this work. Given that each of the Zr-MOFs share the same $Zr_6O_4(OH)_4$-based node, DMMP and DMCP adsorption and reaction most likely occur at undercoordinated zirconium sites. The next section in this Forum Article discusses complementary computational efforts aimed to build upon the experimental findings presented in this section and to better understand both the adsorption and reaction pathways of DMMP, DMCP, and CWAs on Zr-MOFs.

2.1.3. Computational Studies of the Reaction Pathway for DMMP and GB. As with any catalytic process, intimate knowledge of the reaction mechanism at a fully atomistic level can be used to accelerate catalyst development. Consequently, vigorous computational work has been carried out to reveal the reaction mechanism for the degradation of organophosphorus compounds on Zr-MOFs.[28,30,53,54]

The reaction mechanism of nerve-agent hydrolysis by Zr-MOFs involves electrophilic activation of the agent via coordination to the MOF, nucleophilic addition of hydroxide to the phosphorus center of the agent, and elimination of a substituent to yield a less toxic organophosphorus compound (Figure 11). Zr-MOFs are extraordinary materials for hydrolytic removal of nerve agents in part because they present Lewis acidic Zr(IV) sites that enable electrophilic activation of the OP compound upon coordination. Once coordinated, the nerve agent undergoes hydrolysis via hydroxide addition followed by elimination of an −X substituent (X = F or OR, where R is an alkyl group, depending on the nerve agent or mimic). The source of hydroxide might vary according to the conditions. Thus, in buffer solution, OH is provided by the buffer medium,[54] at the gas−solid interface under conditions of high relative humidity by ambient water,[53] and in dry conditions characteristic of ultrahigh-vacuum environments by a hydroxide ligand in a Zr center adjacent to the nerve-agent coordination site.[28,30] The addition of hydroxide to the tetrahedral phosphorus center of the nerve agent generates a pentacoordinated phosphorus intermediate that undergoes

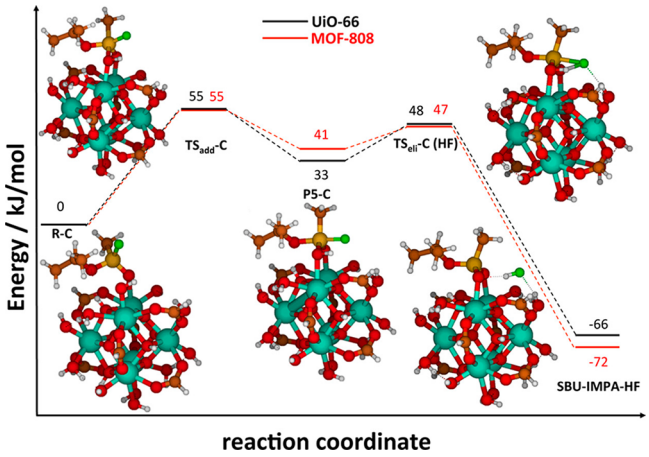

Figure 11. Potential energy diagram for the central steps of the reaction mechanism of GB hydrolysis with the secondary building units (SBUs) of dry UiO-66 (black trace) and MOF-808 (red) along the lowest-energy branch of the C approach. Atom colors are as follows: Zr, teal; O, red; C, brown; H, white. Reprinted from Troya, D. Reaction Mechanism of Nerve-Agent Decomposition with Zr-Based Metal Organic Frameworks. *J. Phys. Chem. C* **2016**, *120*, 29312−29323 (ref 28). Copyright 2016 American Chemical Society.

https://dx.doi.org/10.1021/acsami.9b20833
ACS Appl. Mater. Interfaces 2020, 12, 14641−14661

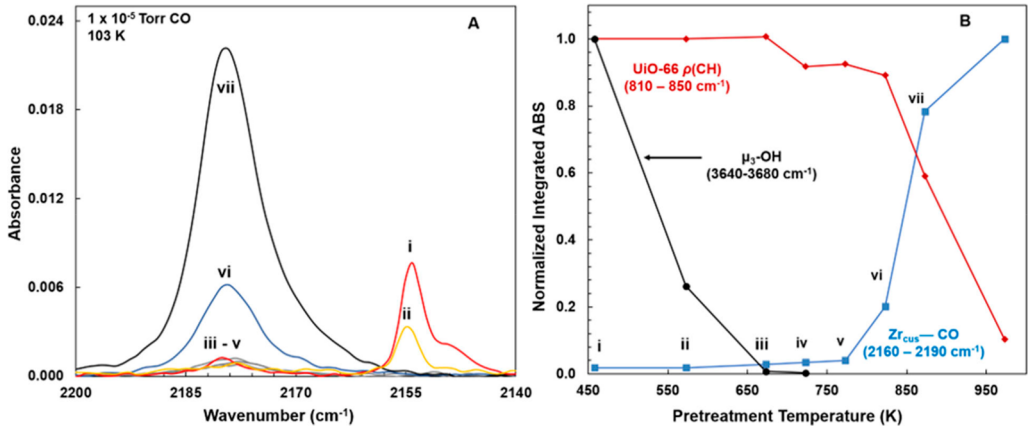

Figure 12. Probing the concentration of missing linkers in UiO-66 as a function of the pretreatment temperature. (A) Infrared spectra recorded during CO adsorption at 103 K. (B) The integrated absorbance of the ρ(CH) modes of UiO-66 (red), μ_3-hydroxyl (black), and the CO (blue) uptake at each corresponding pretreatment temperature. Each data point is normalized relative to the maximum absorbance achieved during thermal treatment for the ρ(CH) modes, μ_3-hydroxyl, and CO bound to Zr, respectively. The labels correspond to the pretreatment temperatures: (i) 448 K, (ii) 573 K, (iii) 673 K, (iv) 723 K, (v) 773 K, (vi) 823 K, and (vii) 873 K. Reprinted from Driscoll, D. M.; Troya, D.; Usov, P. M.; Maynes, A. J.; Morris, A. J.; Morris, J. R. Characterization of Undercoordinated Zr Defect Sites in UiO-66 with Vibrational Spectroscopy of Adsorbed CO. *J. Phys. Chem. C* **2018**, *122*, 14582−14589 (ref 61). Copyright 2018 American Chemical Society.

elimination over low barriers. In GB, the fastest elimination route involves scission of the P−F bond, which removes the biological toxicity of the agent.

An important result of the combined experimental and theoretical work in UHV conditions is that the phosphorus-containing hydrolysis product of the nerve agent remains strongly bound to the MOF, which inhibits further hydrolysis on the same site.[30] Indeed, the interactions between the OP fragment and the Zr-MOF are so strong that they resist thermal treatment at extremely high temperatures such that the Zr-MOF decomposes before the Zr−OP bonds dissociate. Other experiments at the gas−solid interface at ambient pressures have also detected products bound on the Zr-MOF under He flow, suggesting product inhibition in solid Zr-MOF formulations might not be exclusive of vacuum conditions.[39] The strongest-bound products determined by the experiments and calculation feature bidentate binding of the OP fragment that results from nerve-agent hydrolysis to adjacent Zr sites on the MOF,[28,30] which informs the search for alternative materials that isolate the Lewis acid Zr centers. Notwithstanding, new experimental studies that incorporate a solid-state base within MOFs for the hydrolysis of CWA simulants show significant promise in addressing challenges imposed by product inhibition.[6]

2.1.4. Uptake, Diffusion, and Decomposition of 2-CEES within Zr-Based MOFs. In addition to the extensive research that has focused on the development of zirconium-based MOFs for the degradation of nerve agents, recent studies have indicated that these MOFs are also active for the degradation of sulfur mustard (HD). Gil-San-Millan et al. demonstrated that UiO-66-based MOFs are active for the hydrolysis of the HD simulant 2-chloroethyl ethyl sulfide (2-CEES) in solution-phase studies.[55] PCN-222 and NU-1000 post-synthetically modified with photosensitizers have shown the ability to partially oxidize 2-CEES to 2-chloroethyl ethyl sulfoxide under visible light irradiation in solution.[56,57] Motivated by these promising results, we have explored how the Zr-based MOFs interact with HD in the gas phase. Specifically, we are working to understand how HD simulants adsorb within the MOFs and how changes to the MOF structure affect the overall dynamics.

Similar to our studies on the uptake of nerve agents within Zr-based MOFs discussed in a previous section, ongoing studies employ in situ infrared spectroscopy to probe the uptake and transport of the HD simulant 2-CEES in Zr-based MOFs. Upon exposure of the Zr-MOFs to vaporous 2-CEES, the infrared spectra reveal that 2-CEES molecularly adsorbs within the pores of each MOF through the formation of hydrogen bonds with the free hydroxyl groups of the Zr_6 nodes. Previous IR studies of 2-CEES adsorption on amorphous silica,[58] zeolites,[59] and titania−silica powders have indicated that both the sulfur and chlorine moieties in 2-CEES are capable of acting as hydrogen bond acceptors. Our preliminary studies reveal that, in UiO-66, 2-CEES forms hydrogen bonds through the chlorine atoms, whereas in UiO-67 and NU-1000, 2-CEES may form hydrogen bonds through both the sulfur and chlorine atoms, likely due to the less-constrained pore environments of these MOFs. However, similar to the aromatic hydrocarbon system described in a previous section, hydrogen bond breakage appears to not be the diffusion-limiting step for 2-CEES transport through Zr-based MOFs. Instead, the diffusion studies reveal that the pore size(s) of the MOF significantly affects both the rate and activation energy of 2-CEES diffusion through the MOFs: transport was fastest through NU-1000 and slowest in UiO-66. Ongoing efforts are underway to elucidate the diffusion mechanisms and to quantify the rate and energetics of 2-CEES transport through Zr-based MOFs.

2.1.5. Effect of Atmospheric Gases on Zr-MOFs. One of the important aspects of studies on metal−organic frameworks is related to the effect of small gas molecules on the structure and properties of MOFs. The porous MOFs can contain various possible adsorption sites, such as organic linkers, metal nodes, or additional functional groups introduced via post-synthesis modifications.[60] Studies have shown that sorption or separation performance can be improved by tuning reactive metal centers or functionalized ligands that bind to gas molecules. Designing the optimal material for selective gas adsorption, separation, or sensing requires identification of the specific gas adsorption sites as well as transport properties of the porous material. Experimental gas sorption studies of

https://dx.doi.org/10.1021/acsami.9b20833
ACS Appl. Mater. Interfaces 2020, 12, 14641−14661

MOFs usually focus on gas isothermal measurements that, while providing the necessary information on the overall gas uptake and framework behavior upon gas loading, yield limited information on the mechanism of gas adsorption. In our research, we have focused on using *in situ* infrared spectroscopy as well as X-ray diffraction and theoretical calculations that contribute to our understanding of the specific interactions responsible for enhanced adsorption and selectivity and can assist with new synthetic targets for various gas separation processes.

Due to their porous nature and ultrahigh surface areas, MOFs have been proposed in a vast array of applications, among which CO_2 sequestration is one of the most studied. In our work, we focused on the water-stable UiO-66.[60] The structure of UiO-66 is especially interesting as it contains Brønsted acidic and Lewis acidic sites that play an important role in sorption, separation, and potential catalytic processes involving small gaseous molecules. We have determined the CO_2 binding locations and adsorption enthalpies using in situ infrared spectroscopic techniques coupled with DFT. Two unique CO_2 binding motifs in UiO-66 were identified through differing vibrational frequencies of the asymmetric OCO stretching mode. The higher-energy binding appears between μ_3-OH and CO_2 via hydrogen bonding on the MOF nodes with an enthalpy of -38.0 ± 1.5 kJ/mol. The second type of adsorption site that is located within pore space of the MOF stabilized CO_2 molecules through dispersion forces with an enthalpy of adsorption of -30.2 ± 1.3 kJ/mol. Thus, our results show that, in order to optimize the CO_2 adsorption performance, UiO-66 should not be treated beyond the temperature of 573 K because it leads to dehydroxylation and removal of higher-energy adsorption sites.[60]

We used a similar protocol to further explore CO adsorption on both the hydroxylated and dehydroxylated forms of UiO-66 at varying degrees of defect density within the MOF.[61,62] The unique vibrational character of adsorbed CO not only allows for one to probe the molecular nature of acidic sites[61] but also provides the thermodynamics of CO uptake and transport within materials. Two unique binding configurations, both between CO and the μ_3-OH groups of the hydroxylated MOF, were identified on the basis of differing stretching vibrations of CO_{ads} when interacting through the C and O atoms of the molecule (2152 and 2124 cm^{-1}, respectively) (Figure 12). Variable temperature infrared spectroscopy (VTIR) was employed to attain energetics of CO adsorption (17 kJ/mol) and isomerization from the carbonyl to the isocarbonyl configuration (4 kJ/mol). Results suggest that CO−hydroxyl interactions, while weak in nature, play a critical role in CO adsorption within the confined pore environment of UiO-66. Following dehydroxylation of UiO-66, both CO binding geometries are absent, confirming the significance of the hydroxyl−CO interactions to the sorption of carbon monoxide within UiO-66.

Upon sequential heat treatments to 973 K, a new IR feature at 2179 cm^{-1} appeared following the dehydroxylation (Figure 12). The new IR feature at 2179 cm^{-1} was assigned to the excitation of the vibrational motion of CO adsorbed to a coordinatively unsaturated Zr atom at a missing-linker defect site.[63] Each subsequent heat treatment yielded further breakdown of the MOF structure via the removal of organic linkers until the entire MOF was found to have collapsed near 973 K. Confirmation of the CO−Zr_{CUS} assignment was attained through quenching of the Lewis acids with D_2O, which was found to block CO uptake. These results display the power of CO as a probe molecule for characterizing defect sites within MOFs. In addition, the CO and CO_2 studies demonstrate that the VTIR methods provide experimental benchmarks for computational-based studies on small molecule−hydroxyl interactions within MOFs.

As discussed above, we explored how atmospheric gases can influence sarin decontamination in MOFs. In our work, we reported the capture and hydrolysis of a nerve-agent simulant, dimethyl methyl phosphonate (DMMP) vapor, by a series of Zr-based MOFs including UiO-66, UiO-67, MOF-808, and NU-1000. By applying several methods such as PXRD, diffuse reflectance infrared Fourier transform spectroscopy (DRIFTS), and EXAFS, we assigned DMMP adsorption sites and proposed the decomposition mechanism.[27] Knowing the mechanism of decomposition in the pristine laboratory conditions (i.e., He carrier gas), we explored further if the same characteristics were observed if MOFs are exposed to simulant vapor in ambient air. Our results suggest that indeed DMMP enters the pores of activated MOFs, even in the presence of humidity or other ambient gases. Those preliminary results compelled us to explore the effect of ambient gases, specifically CO_2, on the DMMP adsorption and decomposition in a more in-depth study.

We combined in situ FTIR, DRIFTS, synchrotron PXRD, and theoretical calculations to determine how CO_2 binds with MOF-808 and if CO_2 adsorption influences the decomposition of DMMP.[64] We established through VTIR that CO_2 adsorbs within the MOF with an energy of -32.2 ± 1.8 kJ/mol. In situ synchrotron X-ray diffraction results show that CO_2 is located inside the tetrahedral pores, stabilized through dispersion interactions with the pore walls. When CO_2 is introduced to MOF-808 together with DMMP, it leads to the formation of carbonate species as is evident from in situ DRIFTS measurements. The reaction with CO_2 also appears to hinder the decomposition of DMMP until the carbonate formation is complete. The analysis of the kinetics of the reaction suggested that CO_2 accelerates the desorption of bound DMMP and decomposition of MMPA (the reaction byproduct).

2.2. Polyoxometalates. As mentioned above, POMs are another class of highly tunable materials that catalyze the decomposition of CWAs.[38,65] However, key mechanistic details of these catalytic reactions under varying environmental conditions remain unsolved. The next several sections highlight our efforts to understand the surface chemistry that occurs upon vapor-phase exposure of CWA and CWA simulants with and without the presence of ambient gases on two promising POM materials: polyoxoniobate, $Cs_8[Nb_6O_{19}]$, and zirconium-containing POM, $(Et_2NH_2)_8[(\alpha\text{-}PW_{11}O_{39}Zr(\mu\text{-}OH)(H_2O))_2]\cdot 7H_2O$ (referred herein as "Zr-POM").[39,66−68,70]

2.2.1. DMMP Uptake and Decomposition on a Nb_6-Based POM. Wang et al.[36] revealed atomic-level details of the interaction between the Lindqvist polyoxoniobate, $Cs_8Nb_6O_{19}$, and DMMP, by correlating complementary *in situ* measurements, a combination of Raman and synchrotron-based X-ray absorption fine structure (XAFS) spectroscopies with X-ray diffraction (XRD). This is the first time that a structure−activity correlation in POM chemistry has been characterized in situ utilizing three types of complementary measurements performed under nearly identical operational conditions, enabling direct correlation of results across all experiments. In this work, many atomistic details of the reaction, including the nature of the active sites, their dynamic changes during the

https://dx.doi.org/10.1021/acsami.9b20833
ACS Appl. Mater. Interfaces 2020, 12, 14641−14661

reaction, and the characterization of the intermediates or products, have been experimentally investigated. By detecting the reaction products and correlating the changes in the POM that occurred at the corresponding stage of the reaction, we concluded that the reaction follows a general-base hydrolysis mechanism, where DMMP hydrolytically decomposes via the cleavage of a P−OCH_3 bond and forms methanol and methyl methylphosphonic acid (MMPA). During DMMP decomposition, the $Cs_8Nb_6O_{19}$ substrate is protonated at the Lindqvist unit $[Nb_6O_{19}]^{8-}$ oxygen sites, which induces bond distance disordering and charge redistribution in the solid. The process of protonation, coupled with the irreversible binding of the products, strongly suggests that the CsPONb-based materials for OP decomposition may not be viable without new approaches that address product inhibition.

As a complement to the experimental work, the hydrolysis of sarin and surrogate molecules on the cesium salt of hexaniobate, $Cs_8Nb_6O_{19}$, was also subjected to mechanistic interrogation by computational methods.[36,68] Once nerve-agent hydrolysis was detected experimentally,[69] an important question was whether the mechanism followed a general- or specific-base hydrolysis. In the former, hydroxide is generated from water protonation of the base and is added to the nerve agent in a single step. In specific-base hydrolysis, hydroxide is generated first and then is added to the nerve agent in a subsequent step. The association of the nerve agent to the PONb in solution determined by small-angle X-ray scattering (SAXS)[69] initially suggested a general-base mechanism, and calculations in the solid phase set out to probe this mechanism.

DFT exploration of the reaction mechanism did map out a general-base hydrolysis mechanism in the solid state with sarin.[68] It was shown that GB decomposition by $Cs_8Nb_6O_{19}$ is a multistep process and includes the following elementary steps (see Scheme 1): (a) the adsorption of water and the nerve

Scheme 1. Schematic Presentation of the Mechanism of Sarin (GB) Hydrolysis Promoted by the Polyoxoniobate, $Cs_8Nb_6O_{19}$[a]

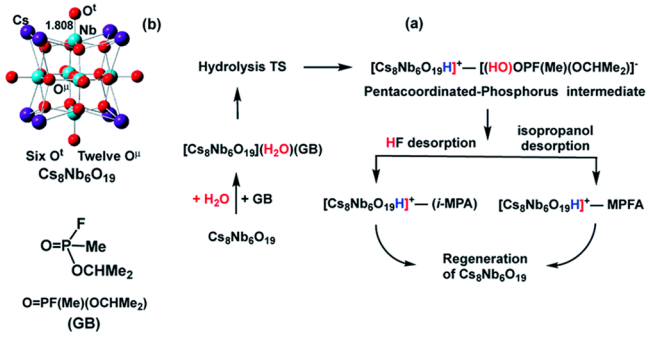

[a]Reprinted with permission from A. L. Kaledin, D. M. Driscoll, D. Troya, D. L. Collins-Wildman, C. L. Hill, J. R. Morris, and D. G. Musaev, *Chem. Sci.*, **2018**, *9*, 2147 (ref 66). Published by The Royal Society of Chemistry.

agent on the most reactive terminal oxo-center (O^t) of the $Cs_8Nb_6O_{19}$ species, (b) concerted dissociation of the adsorbed water molecule on a basic oxygen atom of the polyoxoniobate and nucleophilic addition of the nascent OH group to the phosphorus center of the nerve agent, and (c) rapid reorganization of the resulting pentacoordinated-phosphorus intermediate followed by dissociation of either HF or isopropanol resulting in the formation of POM-bound isopropyl methyl phosphonic acid (*i*-MPA) or methyl phosphonofluoridic acid (MPFA), respectively. The calculations are in full agreement with the experimental work where the phosphonic acids (*i*-MPA) and MPFA are extraordinarily strongly bound to the protonated $[Cs_8Nb_6O_{19}H]^+$ core such that desorption from the solid is not possible upon gentle thermal treatment. This ultimately leads to the poisoning of the CsPONb material. These results suggest full catalyst regeneration might not only require additional treatment but also depend on the nature of counter cations as well as the real-time (ambient) experimental conditions, including the presence of ambient contaminant gases.

2.2.2. Ambient Gas Adsorption on the Nb_6 POM. Comprehensive computational and experimental studies involving NO_2, CO_2, and SO_2 were conducted to elucidate the impacting factors of ambient gas molecules on the structure, stability, and reactivity of this class of POM.[66] These studies revealed that the impact of the diamagnetic CO_2 and SO_2 molecules on $Cs_8Nb_6O_{19}$ is fundamentally different than that of the NO_2 radical. As seen in Table 2, $Cs_8Nb_6O_{19}$

Table 2. Adsorption Energies (Enthalpy, *H*, and Gibbs Free Energy, *G*, in kcal/mol) Defined as Energy Differences of the Complex $Cs_8Nb_6O_{19}$/X and Its Two Separated Fragments, $Cs_8Nb_6O_{19}$ + X, where X = CO_2, NO_2, and SO_2 at 298.15 K and 1 atm[a]

	Δ*H*	Δ*G*
O^t: $Cs_8Nb_6O_{19}$ + CO_2	−29.0	−23.2
O^μ: $Cs_8Nb_6O_{19}$ + CO_2	−16.7	−10.8
O^t: $Cs_8Nb_6O_{19}$ + SO_2	−47.6	−40.3
O^μ: $Cs_8Nb_6O_{19}$ + SO_2	−34.1	−26.6
Cs^N: $Cs_8Nb_6O_{19}$ + NO_2	−22.2	−22.1
O^t: $Cs_8Nb_6O_{19}$ + NO_2	−18.7	−13.9
Cs^N and O^t: $Cs_8Nb_6O_{19}$ + $2NO_2$	−74.6	−58.0
$Cs_8Nb_6O_{19}/CO_2(O^t)$ + H_2O	−22.4	−11.9
$Cs_8Nb_6O_{19}/SO_2(O^t)$ + H_2O	−21.0	−9.7
$Cs_8Nb_6O_{19}$ + H_2O	−23.6	−17.3
$Cs_8Nb_6O_{19}/H_2O$ + GB	−17.4	−4.2
$Cs_8Nb_6O_{19}/H_2O/CO_2(O^t)$ + GB	−17.4	−2.4
$Cs_8Nb_6O_{19}/H_2O/SO_2(O^t)$ + GB	−16.4	−3.7

[a]The superscripts "t" and "μ" indicate the position where the molecule is adsorbed on $Cs_8Nb_6O_{19}$; Cs^N indicates NO_2 adsorption to two Cs counter cations in a symmetric manner. Reprinted with permission from A. L. Kaledin, D. M. Driscoll, D. Troya, D. L. Collins-Wildman, C. L. Hill, J. R. Morris, and D. G. Musaev, *Chem. Sci.*, **2018**, *9*, 2147 (ref 66). Published by The Royal Society of Chemistry.

absorbs SO_2 and, to a lesser extent, CO_2 molecules more strongly than it adsorbs water and sarin (GB) on its reactive O^t center. Calculations also show that, at high ambient gas concentrations, a single $Cs_8Nb_6O_{19}$ species can bind several CO_2 and SO_2 molecules.

IR spectroscopic studies of CO_2 adsorption onto $Cs_8Nb_6O_{19}$ revealed features consistent with a bent structure of the adsorbate at the surface (Figure 13A,i), which is in full agreement with the computational results (Figure 14). Upon evacuation of CO_2 from the chamber, the 1229 cm^{-1} spectroscopic feature associated with a ν_{sym}(C−O) vibration diminishes, indicating that this band corresponds to the vibrational motion of a weakly bound CO_2 species on the surface (Figure 13A,ii); however, the two other features (1659

https://dx.doi.org/10.1021/acsami.9b20833
ACS Appl. Mater. Interfaces 2020, 12, 14641−14661

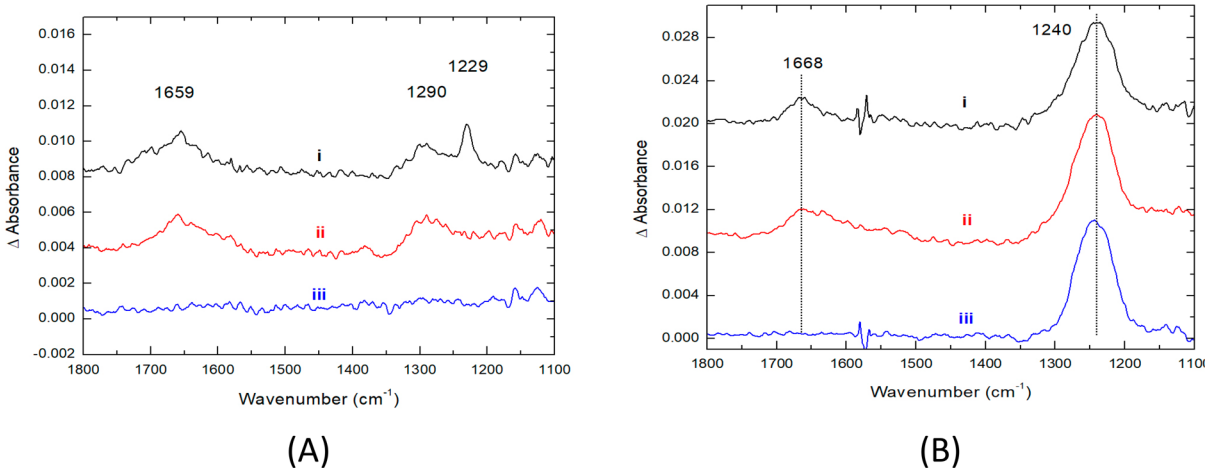

Figure 13. Infrared spectra recorded during and after the adsorption of (A) CO_2 and (B) NO_2 onto $Cs_8Nb_6O_{19}$ at 300 K. (i) Adsorption of 100 mTorr of CO_2 or NO_2. (ii) After CO_2 or NO_2 evacuation. (iii) After CO_2 or NO_2 evacuation and thermal treatment at 423 K. Reprinted with permission from A. L. Kaledin, D. M. Driscoll, D. Troya, D. L. Collins-Wildman, C. L. Hill, J. R. Morris, and D. G. Musaev, *Chem. Sci.*, **2018**, *9*, 2147 (ref 66). Published by The Royal Society of Chemistry.

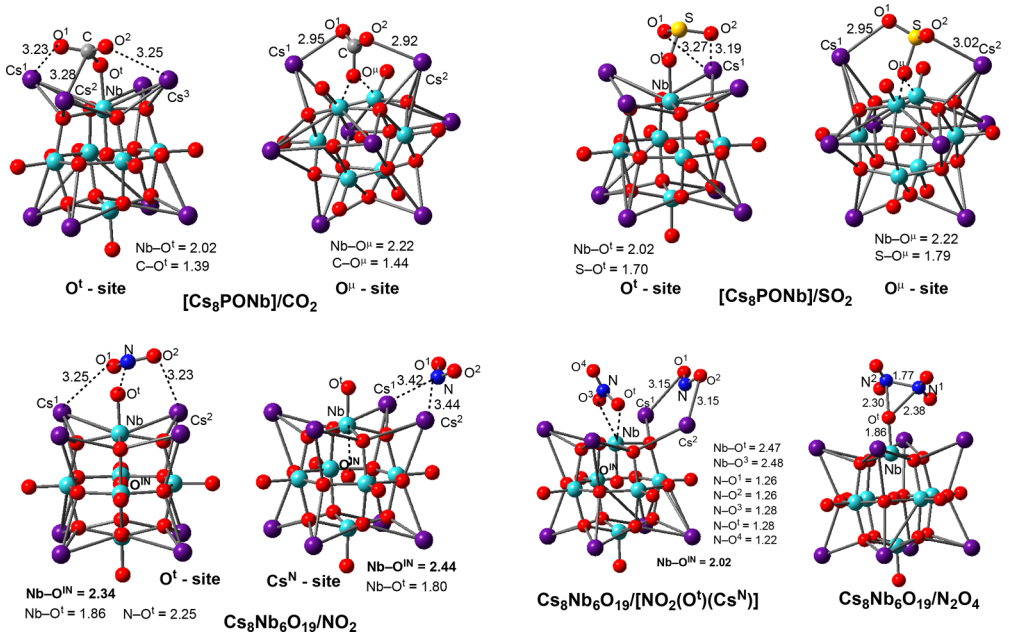

Figure 14. Energetically lowest structures of the ambient gas molecules CO_2, SO_2, and NO_2 adsorption on $Cs_8Nb_6O_{19}$ with their important geometry parameters (in Å). Reprinted with permission from A. L. Kaledin, D. M. Driscoll, D. Troya, D. L. Collins-Wildman, C. L. Hill, J. R. Morris, and D. G. Musaev, *Chem. Sci.*, **2018**, *9*, 2147 (ref 66). Published by The Royal Society of Chemistry.

and 1290 cm^{-1}) persist until heating the $Cs_8Nb_6O_{19}$ sample to 423 K (Figure 13A,iii), which suggests that the molecules responsible for these infrared bands are strongly bound to $Cs_8Nb_6O_{19}$.

Binding of NO_2 radicals to $Cs_8Nb_6O_{19}$ is fundamentally different than that of the diamagnetic CO_2 and SO_2 molecules. At ambient temperatures, a weak coordination of a first NO_2 radical to $Cs_8Nb_6O_{19}$ imparts partial radical character to the polyoxoniobate and promotes coordination of a second NO_2 to the O^t site of the POM to form a stable diamagnetic $Cs_8Nb_6O_{19}/(NO_2)_2$ species. At low temperatures, two NO_2 radicals form a stable dinitrogen tetraoxide (N_2O_4) that weakly interacts with the $Cs_8Nb_6O_{19}$ (Figure 14). The resulting $Cs_8Nb_6O_{19}/[NO_2(Cs^N)NO_2(O^t)]$ species was found to contain the most thermodynamically favorable NO_2 confirmation. In this confirmation, the NO_2 radical binds at the O^t site with an energy that is substantially more favorable than that found for CO_2 interactions (yet slightly weaker than that of SO_2 interactions) at the same location.

Infrared spectroscopic results for the adsorption of NO_2 onto $Cs_8Nb_6O_{19}$ were consistent with the computational studies. Figure 13B shows the spectra for the interaction between NO_2 and $Cs_8Nb_6O_{19}$ where the adsorption of NO_2 on the surface resulted in the formation of two infrared vibrational features. A peak centered at 1240 cm^{-1} (Figure 13B), which persisted at higher temperatures, was assigned to the $Cs_8Nb_6O_{19}/[NO_2(Cs^N)NO_2(O^t)]$ complex. The second feature at 1668 cm^{-1} was consistent with an asymmetric NO stretch originating from the $Cs_8Nb_6O_{19}/N_2O_4$ complex which

https://dx.doi.org/10.1021/acsami.9b20833
ACS Appl. Mater. Interfaces 2020, 12, 14641−14661

transformed into $Cs_8Nb_6O_{19}/[NO_2(Cs^N)NO_2(O^t)]$ upon heating.

The combination of experimental and computational results summarized above suggests that the ambient molecules CO_2, NO_2, and SO_2 may preferentially bind to the NbPOM relative to water and the GB molecules, due to their stronger interactions with POM, both of which are required for hydrolysis (see Table 2). Strongly bound ambient gas molecules may alter the mechanism of sarin hydrolysis by $Cs_8Nb_6O_{19}$ reported earlier by blocking the catalytically active O^t centers and hinder water and sarin coordination. Additionally, the interaction of an ambient gas molecule with $Cs_8Nb_6O_{19}$ may change the electronic properties of the polyoxoniobate, which is expected to impact only the calculated energetics of sarin hydrolysis but will not significantly change the nature of intermediates and transition-state structures reported previously.

2.2.3. Effect of Ambient Gases on the Hydrolysis of Sarin by $Cs_8Nb_6O_{19}$. DFT calculations were performed to test the hypothesis that the presence of ambient gases on $Cs_8Nb_6O_{19}$ affects the hydrolysis mechanism of sarin on $Cs_8Nb_6O_{19}$. Similar to the case without ambient gas molecules,[68] in the presence of CO_2 or SO_2 (X), the GB hydrolysis by $Cs_8Nb_6O_{19}/X$ proceeds via a general-base hydrolysis. Due to the presence of X occupying the active O^t site, water coordinates with $Cs_8Nb_6O_{19}$ via hydrogen bonding to one bridging (O^μ) and one CO (O^1) oxygen atom (instead of O^t) (Figure 15). A concerted hydrolysis of the adsorbed water

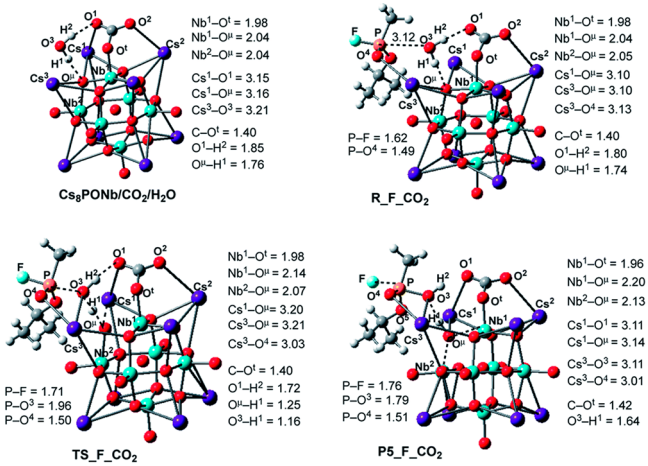

Figure 15. Calculated prereaction complexes, transition state, and product of the GB hydrolysis by $Cs_8Nb_6O_{19}/CO_2$ (i.e., reaction $Cs_8Nb_6O_{19}/CO_2 + H_2O + GB \rightarrow$ R-F_$CO_2 \rightarrow$ TS-F_$CO_2 \rightarrow$ P5-F_CO_2) and their important geometry parameters (in Å). Reprinted with permission from A. L. Kaledin, D. M. Driscoll, D. Troya, D. L. Collins-Wildman, C. L. Hill, J. R. Morris, and D. G. Musaev, *Chem. Sci.*, **2018**, *9*, 2147 (ref 66). Published by The Royal Society of Chemistry.

molecule on a basic oxygen atom of the polyoxoniobate then follows, which results in the nucleophilic addition of a nascent OH group to the phosphorus center of the nerve agent. Decomposition of the ensuing intermediate furnishes HF + i-MPA or isopropanol + MPFA. The resulting phosphonic acids are strongly bound to the solid.

Ultimately, $Cs_8Nb_6O_{19}$ adsorbs the ambient gas molecules CO_2 and SO_2 at its basic O^t (or O^μ) reactive center, which shields them from involvement in the base hydrolysis. As a result, one of the O centers of the coordinated ambient gas molecule becomes an active hydrolysis site. This raises the energy of the stationary points relative to the reactants asymptote and increases the hydrolysis barrier relative to the ambient-gas free $Cs_8Nb_6O_{19}$ (Figure 16). Regeneration of the

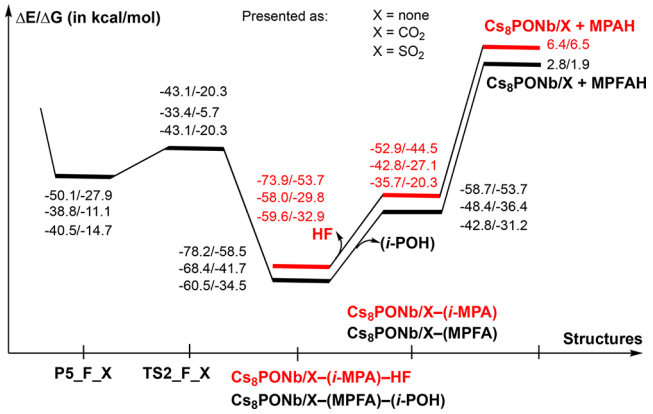

Figure 16. Potential energy profiles of the decomposition reaction of pentacoordinated-phosphorus intermediate P5-F_X, where X = CO_2 and SO_2 at 298.15 K and 1 atm. ΔE and ΔG are the change in electronic and Gibbs free energies and are calculated relative to reactants $Cs_8Nb_6O_{19}/X(O^t) + H_2O$ + GB. Reprinted with permission from A. L. Kaledin, D. M. Driscoll, D. Troya, D. L. Collins-Wildman, C. L. Hill, J. R. Morris, and D. G. Musaev, *Chem. Sci.*, **2018**, *9*, 2147 (ref 66). Published by The Royal Society of Chemistry.

catalyst therefore is a highly endergonic process and is the rate-limiting step for GB hydrolytic decontamination, in both the absence and presence of ambient gas molecules.

2.2.4. Zr-POM Buffer Effects on Chemistry with Simulant. In addition to exploration of the $Cs_8Nb_6O_{19}$ POM, the zirconium-containing POM, $(Et_2NH_2)_8[(\alpha\text{-}PW_{11}O_{39}Zr(\mu\text{-}OH)(H_2O))_2]\cdot 7H_2O$ (Zr-POM) (Figure 17), was extensively

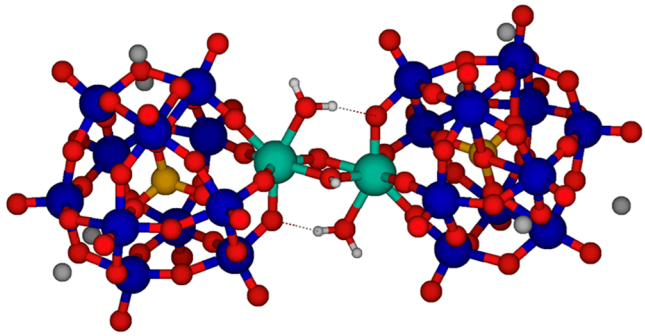

Figure 17. Ball and stick model of the Zr-POM $(Li)_8[[\alpha\text{-}PW_{11}O_{39}Zr(\mu\text{-}OH)(H_2O)]_2]$. Li (gray), W (blue), P (yellow), Zr (teal), O (red), and H (white).

investigated in both homogeneous- and heterogeneous-based catalytic conditions. Due to the heterogeneous nature of Zr-POM and the complexity of its interaction with CWAs/simulants, there are several challenges that limit the understanding of the mechanisms of chemical transformation, including (1) dynamic changes of the structures of both the filtration materials and reactant(s), (2) uncertainty in the nature of the structural/functional units where the reactions occur, (3) scarcity of the experimental methods that are

https://dx.doi.org/10.1021/acsami.9b20833
ACS Appl. Mater. Interfaces 2020, 12, 14641−14661

sensitive to changes that may occur in the several interacting parts of these complex systems, and (4) the need to bring this research to relevant environmental conditions, where the sensitivity of many characterization techniques is particularly limited, and (5) the necessity to evaluate the quality of CWA simulants as adequate model systems.

In an effort to bridge the gap between the CWA hydrolysis studies performed under homogeneous and heterogeneous conditions, several key parameters for solution-phase systems including pH, ionic strength, buffer type, and catalyst and substrate concentrations were evaluated using ^{31}P NMR and DFT calculations for their role in the decomposition mechanism and rate for DMNP reacting with Zr-POM.[70] Specifically, the results of this study reveal the importance of both the identity and concentration of the chosen buffer. DMNP hydrolysis occurred in both acetate- and perchlorate-buffered solutions where the use of acetate yielded a significant enhancement in the rate of decomposition (Figure 18). The

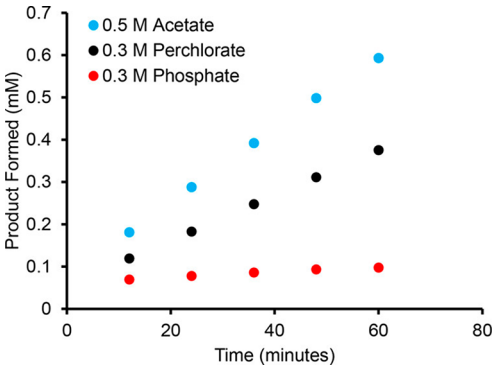

Figure 18. Product formation of DMNP hydrolysis as a function of time in the presence of different anions. Acetate (blue) shows an enhancement over perchlorate (noncoordinating), whereas phosphate (red) exhibits inhibition. Conditions: ionic strength of 0.3 M, 2.5 mM **1**, 10.3 mM DMNP, pH 4.8, pH adjusted with NaOH. Reprinted from Collins-Wildman, D. L.; Kim, M.; Sullivan, K. P.; Plonka, A. M.; Frenkel, A. I.; Musaev, D. G.; Hill, C. L. Buffer-Induced Acceleration and Inhibition in Polyoxometalate-Catalyzed Organophosphorus Ester Hydrolysis. *ACS Catalysis* **2018**, *8*, 7068−7076 (ref 70). Copyright 2018 American Chemical Society.

increased rate was determined to be due to indirect coordination between Zr-POM and the acetate anion, which resulted in a shift in the dimerization mechanism toward the more active monomer form of Zr-POM as well as the acetate acting as a local base. In contrast, the phosphate buffer was found to inhibit the reaction rate due to its direct coordination to the active Zr site on the POM, likely resulting in competition with DMNP for binding with POM.

2.2.5. Mechanistic Insight into Zr-POM Hydrolysis of GB and DMCP. While Zr-POM has been shown to be effective for the hydrolysis of simulants in solution, questions remain regarding its efficacy during gas-phase exposures. In this work, Tian et al.[39] studied the gas−solid reaction between both sarin (GB) and a simulant, dimethyl chlorophosphate (DMCP) with Zr-POM, by utilizing a multimodal approach specific for gas−surface reactions, which includes a set of complementary experimental and theoretical tools: XPS, DRIFTS, synchrotron XRD and XAFS, and DFT calculations. By assembling the tools to probe the atomic-level details of the structural changes in both the Zr-POM and agent/simulant, we concluded that, during GB and DMCP exposures, the Zr-POM dimer transforms to the Zr-POM monomer with a coordinatively unsaturated Zr(IV) center, a key species in the catalytic cycle that binds gaseous GB/DMCP molecules. Specifically, GB and DMCP were found to adsorb through hydrogen bonding at various OH groups on the POM. Both GB and DMCP were observed to mostly physisorb at room temperature, but the presence of asymmetric and symmetric (OPO) stretches clearly indicated some reaction, most likely a nucleophilic (general-base) hydrolysis of the P−F and P−Cl bonds for GB and DMCP, respectively (Figure 19). These results were

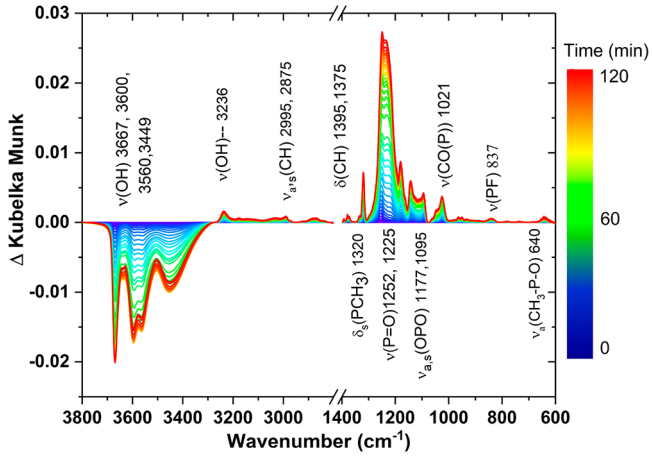

Figure 19. Time-resolved DRIFTS spectra of sarin (GB) uptake onto Zr-POM. Time progresses from the blue to red traces. Clean, unexposed Zr-POM was used as the reference background. Adapted from Tian, Y.; Plonka, A. M.; Ebrahim, A. M.; Palomino, R. M.; Senanayake, S. D.; Balboa, A.; Gordon, W. O.; Troya, D.; Musaev, D. G.; Morris, J. R.; Frenkel, A. I.; et al. Correlated Multimodal Approach Reveals Key Details of Nerve-Agent Decomposition by Single-Site Zr-Based Polyoxometalates. *J. Phys. Chem. Lett.* **2019**, *10*, 2295−2299 (ref 39). Copyright 2019 American Chemical Society.

confirmed by post-dose heating where a loss of the 1252 cm^{-1} P═O stretching mode was observed. Interestingly, for the GB-exposed Zr-POM, a second P═O stretching mode remained, suggesting a more strongly bound product, possibly due to the hydrolysis of the isopropoxy group.

Post-mortem XPS analysis showed that, for the GB-exposed Zr-POM, fluorine remained on the surface, which was not the case for the chlorine of DMCP (Figure 20). We believe these results reveal a key step for GB and DMCP hydrolysis with Zr-POM where the isolation of one Zr atom in Zr-POM following monomerization ameliorates product inhibition because the hydrolysis product does not bind to the catalyst very strongly. In addition, the strong similarity of the GB and DMCP results indicate that DMCP is an adequate simulant for GB adsorption and the reactivity for Zr-POM and can be used as a model system for future studies of CWA deactivation.

Ultimately, the results of these studies provide critical information for understanding the reaction mechanism of CWAs not only in POM-based materials but also in other Zr-based heterogeneous systems such as the Zr-MOFs discussed in the previous sections. Zr-POM can be used to formulate new approaches for reversing the inhibition experienced by both Zr-MOFs and Zr-POM, which ultimately helps guide in the development of next-generation Zr-based CWA hydrolysis catalysts.

https://dx.doi.org/10.1021/acsami.9b20833
ACS Appl. Mater. Interfaces 2020, 12, 14641−14661

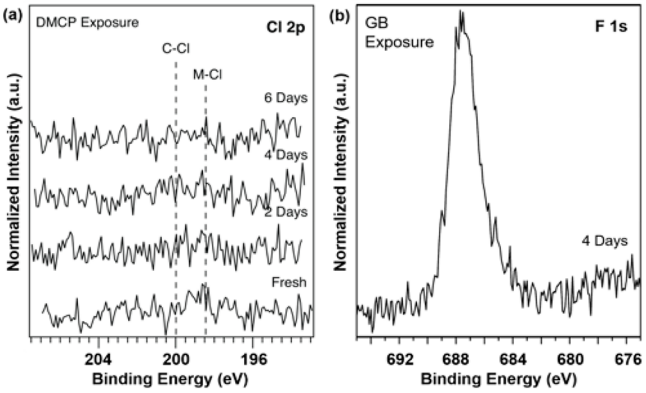

Figure 20. XPS results for (a) DMCP-exposed Zr-POM and (b) GB (sarin)-exposed Zr-POM showing that chlorine is not observed for the DMCP-exposed sample, while F is observed for the GB-exposed POM. Reprinted from Tian, Y.; Plonka, A. M.; Ebrahim, A. M.; Palomino, R. M.; Senanayake, S. D.; Balboa, A.; Gordon, W. O.; Troya, D.; Musaev, D. G.; Morris, J. R.; Frenkel, A. I.; et al. Correlated Multimodal Approach Reveals Key Details of Nerve-Agent Decomposition by Single-Site Zr-Based Polyoxometalates. *J. Phys. Chem. Lett.* **2019**, *10*, 2295−2299 (ref 39). Copyright 2019 American Chemical Society.

3. SCIENTIFIC CHALLENGES

Despite the progress achieved in the mechanistic understanding of CWA capture and/or decomposition in many studies performed in laboratory conditions, there is a further need to determine the impact of real battlefield conditions, such as atmospheric components (e.g., H_2O or CO_2), ambient temperature and pressure, and the gas−solid interface, on the reactions of novel filtration materials with CWAs. The disparities between the studies performed in pristine laboratory conditions and the battlefield environment can include unexpected decomposition performance, lowered dependability, or complications with deployment methods, including how CWA diffusion and reactivities are affected by the final engineered form of the deployed material.[71] The chief challenge in bringing the CWA decontamination research to relevant environmental conditions is the decrease in sensitivity of many characterization techniques at the solid−gas interface at realistic temperature and pressure of the interacting gases. Other challenges in CWA decontamination research include detection and interpretation of the real-time changes of the structures of both the filtration materials and reactants and the complexity of structural/functional units where the reactions occur (examples discussed above demonstrate that the changes may occur in both the CWA molecule and filtration material). The last and, perhaps, the most important challenge, is the need to evaluate the quality of CWA simulants as adequate analogs of real agents.

In this Forum Article, we highlight the solutions that rely on the use of multimodal methods of characterization, conducted under in situ or *in operando* conditions. Multimodal characterization methods, practiced in catalysis science since the 1990s, are applied to the surface reactions at the solid−gas interface in ambient conditions by relying on specialized reaction cell environments that are compatible with several complementary experimental probes, as in the first such experiment of Clausen et al., in which XAFS and XRD studies were combined.[72] Today, the state of the art is conducting catalytic studies in situ or *inoperando*, while combining complementary techniques in a single experiment[73−75] or by using a portable microreactor approach[76−78] in which the same reaction cell is moved from one instrument to another and the reaction products are analyzed to correlate between different experimental probes. The "*in operando*" approach, advanced in the early 2000s,[79] is central for mechanistic studies, where the investigation of active state and active site(s) of a functional material is done by correlating the structural changes with the changes in the material's performance.

As shown above, synchrotron techniques, such as XAS and XRD, play a central role in battlefield-relevant studies of POMs and MOFs during their interaction with CWA simulants, due to the high penetrating power of hard X-rays (hence, the reaction environment can be probed at the conditions of ambient and elevated temperature and pressure). The progress in CWA decontamination studies at the synchrotrons would not be possible without the development of in situ and *in operando* reactors that couple synchrotron techniques (XAS and XRD) with vibrational spectroscopies.[73,80] The combination of XAFS and XRD with DRIFTS and Raman spectroscopy, aided also by the XPS studies, enables the investigation of processes that occur at multiple length scales, such as the uptake of CWA molecules by MOFs and POMs and their interaction with Zr−O moieties.[27,39] The use of the multimodal approach allowed Tian et al. to correlate the results obtained with GB and its simulant, DMCP, using similar techniques (Raman and DRIFTS) to study their interactions with Zr-POMs and address the question of the quality of DMCP as a GB simulant.[39] The combination of multiple probes allowed them to show also that, upon DMCP and GB exposure, the Zr-POM dimer transforms to the Zr-POM monomer with a coordinatively unsaturated Zr(IV) center. The latter is a key species in a catalytic cycle that binds nerve agents and decomposes them via a nucleophilic (general-base) hydrolysis mechanism.[39]

This and other examples described above demonstrate that advanced synchrotron-based, in situ/*in operando* XAS and XRD can be exploited to develop an atomic-level understanding of the binding and reaction of CWAs and impact research on novel filtration materials. Despite their unique advantages for CWA decontamination, synchrotron-based techniques are relatively unexplored by the community because participation in synchrotron research requires expert knowledge of beamline operations and data analysis, access to beamline facilities, and the availability of specialized in situ reactors. The coordination of efforts is needed to assist new users as well as to develop new capabilities for solving CWA decontamination problems using multimodal approaches at the synchrotrons. One possible direction is a synchrotron consortium, modeled after the first such successful example, Synchrotron Catalysis Consortium (SCC), consisting of catalysis researchers from academic, national, and industrial laboratories and established in 2005.[75] Establishing such a consortium for chemical defense (Defense Synchrotron Consortium or DSC) at Brookhaven National Laboratory is in the planning stage. It will be designed to support the research needs of researchers working in CWA filtration material fields at synchrotron beamlines, with specific DSC support for cells and complementary techniques needed to address specialized issues. For example, correlative bulk and surface studies of novel nanocatalysts can be carried out by combined XAS, XRD, DRIFTS, and Raman spectroscopic characterization, as prototyped in several examples described in

https://dx.doi.org/10.1021/acsami.9b20833
ACS Appl. Mater. Interfaces 2020, 12, 14641−14661

detail above. DSC staff will be actively engaged with multiple chemical defense research teams to respond to investigator needs for scientific solutions. Another important mission of the proposed Consortium, training and outreach, to grow the DSC-supported research community, will be performed by providing annual short courses on experimental methods and data analysis and modeling techniques used in the DSC research projects.

4. PERSPECTIVES FOR NEXT-GENERATION SORBENTS: THE PUSH TOWARD TRUE CATALYSIS FOR CWA DESTRUCTION

For over a century, adsorbent-based technologies have been the primary means employed for protection of the warfighter from the threat of chemical warfare exposure. The capture efficiency and selectivity of the adsorbents have evolved with the nature of the chemical threat, such as the chemical's toxicity and physical−chemical properties, which play a major role in affecting the adsorption rate, capacity, decomposition, and retention of the CWA in battlefield environments.[7] Vapor pressure or volatility of a CWA is a key parameter that influences the design of adsorbents and their configuration in protective suits and filters. As previously discussed for CWAs where physical adsorption is dominant (low vapor pressure), the size and number of the adsorbent pores on a volume basis are major design parameters used to engineer protective equipment. For CWAs possessing high vapor pressures, a combination of physical adsorption and adsorbed-phase chemical decomposition is necessary to prevent desorption (off-gassing) into otherwise clean air environments.

In recent decades, the use of CWAs in urban environments has dramatically increased such that it is difficult to adequately understand with a high level of certainty the protection afforded to the warfighter. Military personnel are faced with increasing uncertainty in a complex battlefield environment in which the presence of CWAs can result in a significant impact on operations. Today, there is a concerted effort underway to significantly enhance the protective capabilities of adsorbent-based materials by providing greater adsorption and reactive capacities for a broader spectrum of chemical threats.[7] For example, Zr-based MOFs offer virtually infinite structures for the design against CWAs and emerging hazards, but their exploitation depends critically on understanding the structure−activity relationship for efficient uptake and decomposition of CWAs under realistic battlefield conditions. To achieve these goals, two major research challenges must be addressed. One centers on understanding the innate capabilities and limitations of solid porous materials and the ability to rationally design structural topologies that efficiently adsorb, transport, and diffuse CWAs to highly dispersed active centers. The second is to fully understand the adsorption dynamics of promising materials under realistic battlefield conditions. A key challenge is to bridge the gap between controlled, solution-phase laboratory studies and real-world or battlefield-like conditions by examining agent−material interactions at the gas−solid interface utilizing a multimodal experimental and computational approach. As previously discussed, we have developed a number of in situ and *in operando* techniques that have provided new insight to the dynamical changes of a catalyst during exposure to CWAs and simulants under realistic environmental conditions, such as the presence of humidity, carbon dioxide, sulfur dioxide, nitrogen oxides, and hydrocarbons.[47,48,60−62,66,81]

Unlike bulk amorphous and semicrystalline materials, such as activated carbon and traditional metal oxides, our material research efforts for the past decade have focused on crystalline-based platforms such as MOFs and POMs that possess well-defined periodic topologies and high fractional loading of metal centers (e.g., Zr−O nodes). Here, our aim is to provide a fundamental understanding of adsorption, mass transport, and chemical activity at the molecular level and to provide new insight on how topological parameters of MOFs affect the overall CWA degradation process and thereby to elucidate design rules based on the role of topology for developing porous catalysts with optimized functions.

The next generation of active oxides centers on using highly energetic forms of single atom materials and small clusters to promote stronger binding and molecular dissociation without the dependency on external energy sources (i.e., thermal, light). The ultimate small-size limit for metal particles is the single-atom catalyst (SAC), which contains isolated metal atoms singly dispersed on oxide supports. SACs maximize the efficiency of the metal atom used, which is particularly important for supported metal catalysts. Moreover, with well-defined and uniform single-atom dispersion, SACs offer a great potential for achieving high stability, selectivity toward distinct classes of CWAs, and turnover numbers that reflect true catalyst behavior. Our research on SACs is focused on extending the reaction envelope of oxide platforms such as MOFs and POMs with the aim to advance our understanding on how to design new forms of highly active materials that exhibit new chemistries to adsorb, transport, and decompose CWAs. This research builds on the current knowledge of MOF, POM, and traditional metal oxide activities with the aim to provide tunable properties to promote highly efficient capture and decomposition of adsorbed CWAs.

5. CONCLUSION

Rational development of improved catalysts requires an understanding of the limitations and deficiencies of the materials. Our research team utilized a multimodal approach to study fundamental CWA−MOF/POM interactions, including the presence of common ambient gases, at the gas−solid interface. Computation methodologies linked the experimental results to elucidate atomic-scale mechanisms of CWA decomposition and product formation on MOF and POM surfaces. From there, a feedback loop was created where both experimental and computation results directed new synthetic efforts toward the development of improved CWA catalytic materials, which could be fed back for experimental exploration. Finally, experimental results from CWA simulant-based studies guided the testing of live chemical agents on our MOF and POM materials. The knowledge gained using this experimental approach highlighted the importance of bridging the gap between pristine laboratory-based studies and real-world performance. Notably, we revealed that, under vapor-phase exposure of nerve-agent simulants, both Zr-based MOF and POM materials are susceptible to poisoning of the active Zr sites, which through computation methods was determined to be a bidentate-bound phosphonic acid species. These molecular-level details provide the groundwork for developing improved catalytic materials that utilize the promising properties of the reactive Zr sites but are designed to prevent the bidentate coordination between the reaction product and the active site. While significant progress has been made in understanding the behavior of these materials, a

https://dx.doi.org/10.1021/acsami.9b20833
ACS Appl. Mater. Interfaces 2020, 12, 14641−14661

knowledge gap between the performance in the laboratory and that under real world-conditions remains. We believe the wide range of complementary techniques utilized in the above studies provides a tool chest to address these issues in future catalyst development research.

AUTHOR INFORMATION

Corresponding Author

John R. Morris − *Department of Chemistry, Virginia Tech, Blacksburg, Virginia 24061, United States;* orcid.org/0000-0001-9140-5211; Email: jrmorris@vt.edu

Authors

Tyler G. Grissom − *Department of Chemistry, Virginia Tech, Blacksburg, Virginia 24061, United States;* orcid.org/0000-0001-7337-006X

Anna M. Plonka − *Department of Materials Science and Chemical Engineering, Stony Brook University, Stony Brook, New York 11794, United States;* orcid.org/0000-0003-2606-0477

Conor H. Sharp − *Department of Chemistry, Virginia Tech, Blacksburg, Virginia 24061, United States;* orcid.org/0000-0002-5313-0760

Amani M. Ebrahim − *Department of Materials Science and Chemical Engineering, Stony Brook University, Stony Brook, New York 11794, United States*

Yiyao Tian − *Department of Materials Science and Chemical Engineering, Stony Brook University, Stony Brook, New York 11794, United States;* orcid.org/0000-0002-8148-9375

Daniel L. Collins-Wildman − *Department of Chemistry, Emory University, Atlanta, Georgia 30322, United States*

Alexey L. Kaledin − *Cherry L. Emerson Center for Scientific Computation, Emory University, Atlanta, Georgia 30322, United States;* orcid.org/0000-0003-3112-3989

Harrison J. Siegal − *Department of Chemistry, Virginia Tech, Blacksburg, Virginia 24061, United States*

Diego Troya − *Department of Chemistry, Virginia Tech, Blacksburg, Virginia 24061, United States;* orcid.org/0000-0003-4971-4998

Craig L. Hill − *Department of Chemistry, Emory University, Atlanta, Georgia 30322, United States;* orcid.org/0000-0002-5506-9588

Anatoly I. Frenkel − *Department of Materials Science and Chemical Engineering, Stony Brook University, Stony Brook, New York 11794, United States; Chemistry Division, Brookhaven National Laboratory, Upton, New York 11973, United States;* orcid.org/0000-0002-5451-1207

Djamaladdin G. Musaev − *Cherry L. Emerson Center for Scientific Computation, Emory University, Atlanta, Georgia 30322, United States;* orcid.org/0000-0003-1160-6131

Wesley O. Gordon − *U.S. Army Combat Capabilities Development Command Chemical Biological Center, Aberdeen, Maryland 21010, United States;* orcid.org/0000-0001-7766-4102

Christopher J. Karwacki − *U.S. Army Combat Capabilities Development Command Chemical Biological Center, Aberdeen, Maryland 21010, United States*

Mark B. Mitchell − *Department of Chemistry, Kennesaw State University, Kennesaw, Georgia 30144, United States*

Complete contact information is available at: https://pubs.acs.org/10.1021/acsami.9b20833

Notes

The views and conclusions contained herein are those of the authors and should not be interpreted as necessarily representing the official policies or endorsements, either expressed or implied, of the ARO, DOE, DOD, or the U.S. Government. The U.S. Government is authorized to reproduce and distribute reprints for Governmental purposes notwithstanding any copyright annotation thereon.

The authors declare no competing financial interest.

ACKNOWLEDGMENTS

This work is supported by the U.S. Army Research Laboratory and the U.S. Army Research Office under grant number W911NF-15-2-0107. We thank the Defense Threat Reduction Agency for support under program CB3587. Reaction tests at Brookhaven National Laboratory's Chemistry Division were made possible due to the Laboratory Directed Research and Development Program through the LDRD 18-047 fund to A.I.F. This research used beamline 28-ID-2 (XPD) of the National Synchrotron Light Source II, a U.S. DOE Office of Science User Facility operated for the DOE Office of Science by Brookhaven National Laboratory under Contract No. DE-SC0012704. This research used beamlines 17-BM and 9-BM of the Advanced Photon Source at Argonne National Laboratory and BL2-2 beamline of the Stanford Synchrotron Radiation Lightsource of the SLAC National Laboratory. Uses of the Argonne Advanced Photon Source and Stanford Synchrotron Radiation Lightsource were supported by DOE under Contract Nos. DE-AC02-06CH11357 and DE-AC02-76SF00515, respectively. We acknowledge Cherry L. Emerson Center for Scientific Computation at Emory University and the Advanced Research Computing at Virginia Tech for providing computational resources and technical support.

REFERENCES

(1) Yang, Y. C.; Baker, J. A.; Ward, J. R. Decontamination of Chemical Warfare Agents. *Chem. Rev.* **1992**, *92*, 1729−1743.

(2) Love, A. H.; Bailey, C. G.; Hanna, M. L.; Hok, S.; Vu, A. K.; Reutter, D. J.; Raber, E. Efficacy of Liquid and Foam Decontamination Technologies for Chemical Warfare Agents on Indoor Surfaces. *J. Hazard. Mater.* **2011**, *196*, 115−122.

(3) Kumar, V.; Goel, R.; Chawla, R.; Silambarasan, M.; Sharma, R. Chemical, Biological, Radiological, and Nuclear Decontamination: Recent Trends and Future Perspective. *J. Pharm. BioAllied Sci.* **2010**, *2*, 220−238.

(4) Huynh, K.; Holdren, S.; Hu, J.; Wang, L.; Zachariah, M. R.; Eichhorn, B. W. Dimethyl Methylphosphonate Adsorption Capacities and Desorption Energies on Ordered Mesoporous Carbons. *ACS Appl. Mater. Interfaces* **2017**, *9*, 40638−40644.

(5) Colón-Ortiz, J.; Landers, J. M.; Gordon, W. O.; Balboa, A.; Karwacki, C. J.; Neimark, A. V. Disordered Mesoporous Zirconium (Hydr)oxides for Decomposition of Dimethyl Chlorophosphate. *ACS Appl. Mater. Interfaces* **2019**, *11*, 17931−17939.

(6) Chen, Z.; Ma, K.; Mahle, J. J.; Wang, H.; Syed, Z. H.; Atilgan, A.; Chen, Y.; Xin, J. H.; Islamoglu, T.; Peterson, G. W.; Farha, O. K. Integration of Metal−Organic Frameworks on Protective Layers for Destruction of Nerve Agents under Relevant Conditions. *J. Am. Chem. Soc.* **2019**, *141*, 20016−20021.

(7) DeCoste, J. B.; Peterson, G. W. Metal-Organic Frameworks for Air Purification of Toxic Chemicals. *Chem. Rev.* **2014**, *114*, 5695−5727.

(8) Kim, K.; Tsay, O. G.; Atwood, D. A.; Churchill, D. G. Destruction and Detection of Chemical Warfare Agents. *Chem. Rev.* **2011**, *111*, 5345−5403.

(9) Thomas, J. M.; Williams, R. J. P. Catalysis: Principles, Progress, Prospects. *Philos. Trans. R. Soc., A* **2005**, *363*, 765−791.
(10) Jencks, W. P. *Catalysis in Chemistry and Enzymology*; McGraw-Hill: New York, NY, 1969.
(11) Moon, S.-Y.; Wagner, G. W.; Mondloch, J. E.; Peterson, G. W.; DeCoste, J. B.; Hupp, J. T.; Farha, O. K. Effective, Facile, and Selective Hydrolysis of the Chemical Warfare Agent VX Using Zr-6-Based Metal-Organic Frameworks. *Inorg. Chem.* **2015**, *54*, 10829−10833.
(12) Agrawal, M.; Sava Gallis, D. F.; Greathouse, J. A.; Sholl, D. S. How Useful Are Common Simulants of Chemical Warfare Agents at Predicting Adsorption Behavior? *J. Phys. Chem. C* **2018**, *122*, 26061−26069.
(13) Neufeld, M. J.; Ware, B. R.; Lutzke, A.; Khetani, S. R.; Reynolds, M. M. Water-Stable Metal−Organic Framework/Polymer Composites Compatible with Human Hepatocytes. *ACS Appl. Mater. Interfaces* **2016**, *8*, 19343−19352.
(14) Wang, P.-L.; Xie, L.-H.; Joseph, E. A.; Li, J.-R.; Su, X.-O.; Zhou, H.-C. Metal−Organic Frameworks for Food Safety. *Chem. Rev.* **2019**, *119*, 10638.
(15) Neufeld, M. J.; Lutzke, A.; Tapia, J. B.; Reynolds, M. M. Metal−Organic Framework/Chitosan Hybrid Materials Promote Nitric Oxide Release from S-Nitrosoglutathione in Aqueous Solution. *ACS Appl. Mater. Interfaces* **2017**, *9*, 5139−5148.
(16) Lai, Z.; Bonilla, G.; Diaz, I.; Nery, J. G.; Sujaoti, K.; Amat, M. A.; Kokkoli, E.; Terasaki, O.; Thompson, R. W.; Tsapatsis, M.; Vlachos, D. G. Microstructural Optimization of a Zeolite Membrane for Organic Vapor Separation. *Science* **2003**, *300*, 456.
(17) Bobbitt, N. S.; Mendonca, M. L.; Howarth, A. J.; Islamoglu, T.; Hupp, J. T.; Farha, O. K.; Snurr, R. Q. Metal-Organic Frameworks for the Removal of Toxic Industrial Chemicals and Chemical Warfare Agents. *Chem. Soc. Rev.* **2017**, *46*, 3357−3385.
(18) Peterson, G. W.; Destefano, M. R.; Garibay, S. J.; Ploskonka, A.; McEntee, M.; Hall, M.; Karwacki, C. J.; Hupp, J. T.; Farha, O. K. Optimizing Toxic Chemical Removal through Defect-Induced UiO-66-NH_2 Metal-Organic Framework. *Chem. - Eur. J.* **2017**, *23*, 15913−15916.
(19) Chung, Y. G.; Camp, J.; Haranczyk, M.; Sikora, B. J.; Bury, W.; Krungleviciute, V.; Yildirim, T.; Farha, O. K.; Sholl, D. S.; Snurr, R. Q. Computation-Ready, Experimental Metal−Organic Frameworks: A Tool To Enable High-Throughput Screening of Nanoporous Crystals. *Chem. Mater.* **2014**, *26*, 6185−6192.
(20) Saha, D.; Deng, S. Ammonia Adsorption and its Effects on Framework Stability of MOF-5 and MOF-177. *J. Colloid Interface Sci.* **2010**, *348*, 615−620.
(21) Liu, J.; Wei, Y.; Li, P.; Zhao, Y.; Zou, R. Selective H_2S/CO_2 Separation by Metal−Organic Frameworks Based on Chemical-Physical Adsorption. *J. Phys. Chem. C* **2017**, *121*, 13249−13255.
(22) Cavka, J. H.; Jakobsen, S.; Olsbye, U.; Guillou, N.; Lamberti, C.; Bordiga, S.; Lillerud, K. P. A New Zirconium Inorganic Building Brick Forming Metal Organic Frameworks with Exceptional Stability. *J. Am. Chem. Soc.* **2008**, *130*, 13850−13851.
(23) Mondloch, J. E.; Bury, W.; Fairen-Jimenez, D.; Kwon, S.; DeMarco, E. J.; Weston, M. H.; Sarjeant, A. A.; Nguyen, S. T.; Stair, P. C.; Snurr, R. Q.; Farha, O. K.; Hupp, J. T. Vapor-Phase Metalation by Atomic Layer Deposition in a Metal-Organic Framework. *J. Am. Chem. Soc.* **2013**, *135*, 10294−10297.
(24) Furukawa, H.; Gandara, F.; Zhang, Y. B.; Jiang, J. C.; Queen, W. L.; Hudson, M. R.; Yaghi, O. M. Water Adsorption in Porous Metal-Organic Frameworks and Related Materials. *J. Am. Chem. Soc.* **2014**, *136*, 4369−4381.
(25) Peterson, G. W.; Moon, S. Y.; Wagner, G. W.; Hall, M. G.; DeCoste, J. B.; Hupp, J. T.; Farha, O. K. Tailoring the Pore Size and Functionality of UiO-Type Metal-Organic Frameworks for Optimal Nerve Agent Destruction. *Inorg. Chem.* **2015**, *54*, 9684−9686.
(26) Ruffley, J. P.; Goodenough, I.; Luo, T.-Y.; Richard, M.; Borguet, E.; Rosi, N. L.; Johnson, J. K. Design, Synthesis, and Characterization of Metal−Organic Frameworks for Enhanced Sorption of Chemical Warfare Agent Simulants. *J. Phys. Chem. C* **2019**, *123*, 19748−19758.
(27) Plonka, A. M.; Wang, Q.; Gordon, W. O.; Balboa, A.; Troya, D.; Guo, W.; Sharp, C. H.; Senanayake, S. D.; Morris, J. R.; Hill, C. L.; Frenkel, A. I. In Situ Probes of Capture and Decomposition of Chemical Warfare Agent Simulants by Zr-Based Metal Organic Frameworks. *J. Am. Chem. Soc.* **2017**, *139*, 599−602.
(28) Troya, D. Reaction Mechanism of Nerve-Agent Decomposition with Zr-Based Metal Organic Frameworks. *J. Phys. Chem. C* **2016**, *120*, 29312−29323.
(29) Wang, H.; Mahle, J. J.; Tovar, T. M.; Peterson, G. W.; Hall, M. G.; DeCoste, J. B.; Buchanan, J. H.; Karwacki, C. J. Solid-Phase Detoxification of Chemical Warfare Agents using Zirconium-Based Metal Organic Frameworks and the Moisture Effects: Analyze via Digestion. *ACS Appl. Mater. Interfaces* **2019**, *11*, 21109−21116.
(30) Wang, G.; Sharp, C.; Plonka, A. M.; Wang, Q.; Frenkel, A. I.; Guo, W.; Hill, C.; Smith, C.; Kollar, J.; Troya, D.; Morris, J. R. Mechanism and Kinetics for Reaction of the Chemical Warfare Agent Simulant, DMMP(g), with Zirconium(IV) MOFs: An Ultrahigh-Vacuum and DFT Study. *J. Phys. Chem. C* **2017**, *121*, 11261−11272.
(31) Harvey, J. A.; McEntee, M. L.; Garibay, S. J.; Durke, E. M.; DeCoste, J. B.; Greathouse, J. A.; Sava Gallis, D. F. Spectroscopically Resolved Binding Sites for the Adsorption of Sarin Gas in a Metal−Organic Framework: Insights beyond Lewis Acidity. *J. Phys. Chem. Lett.* **2019**, *10*, 5142−5147.
(32) Hill, C. L. Introduction: PolyoxometalatesMulticomponent Molecular Vehicles To Probe Fundamental Issues and Practical Problems. *Chem. Rev.* **1998**, *98*, 1−2.
(33) Kozhevnikov, I. V. Catalysis by Heteropoly Acids and Multicomponent Polyoxometalates in Liquid-Phase Reactions. *Chem. Rev.* **1998**, *98*, 171−198.
(34) Dong, J.; Lv, H.; Sun, X.; Wang, Y.; Ni, Y.; Zou, B.; Zhang, N.; Yin, A.; Chi, Y.; Hu, C. A Versatile Self-Detoxifying Material Based on Immobilized Polyoxoniobate for Decontamination of Chemical Warfare Agent Simulants. *Chem. - Eur. J.* **2018**, *24*, 19208−19215.
(35) Li, X.; Dong, J.; Liu, H.; Sun, X.; Chi, Y.; Hu, C. Recoverable Amphiphilic Polyoxoniobates Catalyzing Oxidative and Hydrolytic Decontamination of Chemical Warfare Agent Simulants in Emulsion. *J. Hazard. Mater.* **2018**, *344*, 994−999.
(36) Wang, Q.; Chapleski, R. C., Jr.; Plonka, A. M.; Gordon, W. O.; Guo, W.; Thuy-Duong, N.-P.; Sharp, C. H.; Marinkovic, N. S.; Senanayake, S. D.; Morris, J. R.; Hill, C. L.; Troya, D.; Frenkel, A. I. Atomic-Level Structural Dynamics of Polyoxoniobates during DMMP Decomposition. *Sci. Rep.* **2017**, *7*, 773.
(37) Dong, J.; Hu, J.; Chi, Y.; Lin, Z.; Zou, B.; Yang, S.; Hill, C. L.; Hu, C. A Polyoxoniobate−Polyoxovanadate Double-Anion Catalyst for Simultaneous Oxidative and Hydrolytic Decontamination of Chemical Warfare Agent Simulants. *Angew. Chem., Int. Ed.* **2017**, *56*, 4473−4477.
(38) Guo, W.; Lv, H.; Sullivan, K. P.; Gordon, W. O.; Balboa, A.; Wagner, G. W.; Musaev, D. G.; Bacsa, J.; Hill, C. L. Broad-Spectrum Liquid- and Gas-Phase Decontamination of Chemical Warfare Agents by One-Dimensional Heteropolyniobates. *Angew. Chem., Int. Ed.* **2016**, *55*, 7403−7407.
(39) Tian, Y.; Plonka, A. M.; Ebrahim, A. M.; Palomino, R. M.; Senanayake, S. D.; Balboa, A.; Gordon, W. O.; Troya, D.; Musaev, D. G.; Morris, J. R.; Mitchell, M. B.; Collins-Wildman, D. L.; Hill, C. L.; Frenkel, A. I. Correlated Multimodal Approach Reveals Key Details of Nerve-Agent Decomposition by Single-Site Zr-Based Polyoxometalates. *J. Phys. Chem. Lett.* **2019**, *10*, 2295−2299.
(40) Hou, Y.; An, H.; Zhang, Y.; Hu, T.; Yang, W.; Chang, S. Rapid Destruction of Two Types of Chemical Warfare Agent Simulants by Hybrid Polyoxomolybdates Modified by Carboxylic Acid Ligands. *ACS Catal.* **2018**, *8*, 6062−6069.
(41) Hou, Y.; An, H.; Chang, S.; Zhang, J. Versatile Catalysts Constructed from Hybrid Polyoxomolybdates for Simultaneously Detoxifying Sulfur Mustard and Organophosphate Simulants. *Catal. Sci. Technol.* **2019**, *9*, 2445−2455.
(42) Jang, Y. J.; Kim, K.; Tsay, O. G.; Atwood, D. A.; Churchill, D. G. Update 1 of: Destruction and Detection of Chemical Warfare Agents. *Chem. Rev.* **2015**, *115*, PR1−PR76.

https://dx.doi.org/10.1021/acsami.9b20833
ACS Appl. Mater. Interfaces 2020, 12, 14641−14661

(43) Buru, C. T.; Li, P.; Mehdi, B. L.; Dohnalkova, A.; Platero-Prats, A. E.; Browning, N. D.; Chapman, K. W.; Hupp, J. T.; Farha, O. K. Adsorption of a Catalytically Accessible Polyoxometalate in a Mesoporous Channel-type Metal-Organic Framework. *Chem. Mater.* **2017**, *29*, 5174−5181.
(44) Johnson, R. P.; Hill, C. L. Polyoxometalate Oxidation of Chemical Warfare Agent Simulants in Fluorinated Media. *J. Appl. Toxicol.* **1999**, *19*, S71−S75.
(45) Rhule, J. T.; Neiwert, W. A.; Hardcastle, K. I.; Do, B. T.; Hill, C. L. $Ag_5PV_2Mo_{10}O_{40}$, a Heterogeneous Catalyst for Air-Based Selective Oxidation at Ambient Temperature. *J. Am. Chem. Soc.* **2001**, *123*, 12101−12102.
(46) Kim, S.; Byl, O.; Liu, J. C.; Johnson, J. K.; Yates, J. T. Spectroscopic Measurement of Diffusion Kinetics through Subnanometer and Larger Al_2O_3 Particles by a New Method: The Interaction of 2-Chloroethylethyl Sulfide with Gamma-Al_2O_3. *J. Phys. Chem. B* **2006**, *110*, 9204−9210.
(47) Sharp, C. H.; Abelard, J.; Plonka, A. M.; Guo, W.; Hill, C. L.; Morris, J. R. Alkane−OH Hydrogen Bond Formation and Diffusion Energetics of *n*-Butane within UiO-66. *J. Phys. Chem. C* **2017**, *121*, 8902−8906.
(48) Grissom, T. G.; Sharp, C. H.; Usov, P. M.; Troya, D.; Morris, A. J.; Morris, J. R. Benzene, Toluene, and Xylene Transport through UiO-66: Diffusion Rates, Energetics, and the Role of Hydrogen Bonding. *J. Phys. Chem. C* **2018**, *122*, 16060−16069.
(49) Rives, S.; Jobic, H.; Kolokolov, D. I.; Gabrienko, A. A.; Stepanov, A. G.; Ke, Y.; Frick, B.; Devic, T.; Férey, G.; Maurin, G. Diffusion of Xylene Isomers in the MIL-47(V) MOF Material: A Synergic Combination of Computational and Experimental Tools. *J. Phys. Chem. C* **2013**, *117*, 6293−6302.
(50) Lennox, M. J.; Duren, T. Understanding the Kinetic and Thermodynamic Origins of Xylene Separation in UiO-66(Zr) via Molecular Simulation. *J. Phys. Chem. C* **2016**, *120*, 18651−18658.
(51) Agrawal, M.; Boulfelfel, S. E.; Sava Gallis, D. F.; Greathouse, J. A.; Sholl, D. S. Determining Diffusion Coefficients of Chemical Warfare Agents in Metal−Organic Frameworks. *J. Phys. Chem. Lett.* **2019**, *10*, 7823−7830.
(52) Head, A. R.; Tang, X.; Hicks, Z.; Wang, L.; Bleuel, H.; Holdren, S.; Trotochaud, L.; Yu, Y.; Kyhl, L.; Karslıoğlu, O.; Fears, K.; Owrutsky, J.; Zachariah, M.; Bowen, K. H.; Bluhm, H. Thermal Desorption of Dimethyl Methylphosphonate from MoO3 AU. *Catal. Struct. React.* **2017**, *3*, 112−118.
(53) Momeni, M. R.; Cramer, C. J. Dual Role of Water in Heterogeneous Catalytic Hydrolysis of Sarin by Zirconium-Based Metal-Organic Frameworks. *ACS Appl. Mater. Interfaces* **2018**, *10*, 18435−18439.
(54) Chen, H.; Mendonca, M. L.; Snurr, R. Q.; et al. Insights into Catalytic Hydrolysis of Organophosphate Warfare Agents by Metal−Organic Framework NU-1000. *J. Phys. Chem. C* **2018**, *122*, 12362−12368.
(55) Gil-San-Millan, R.; López-Maya, E.; Hall, M.; Padial, N. M.; Peterson, G. W.; DeCoste, J. B.; Rodríguez-Albelo, L. M.; Oltra, J. E.; Barea, E.; Navarro, J. A. R. Chemical Warfare Agents Detoxification Properties of Zirconium Metal−Organic Frameworks by Synergistic Incorporation of Nucleophilic and Basic Sites. *ACS Appl. Mater. Interfaces* **2017**, *9*, 23967−23973.
(56) Howarth, A. J.; Buru, C. T.; Liu, Y.; Ploskonka, A. M.; Hartlieb, K. J.; McEntee, M.; Mahle, J. J.; Buchanan, J. H.; Durke, E. M.; Al-Juaid, S. S.; Stoddart, J. F.; DeCoste, J. B.; Hupp, J. T.; Farha, O. K. Postsynthetic Incorporation of a Singlet Oxygen Photosensitizer in a Metal−Organic Framework for Fast and Selective Oxidative Detoxification of Sulfur Mustard. *Chem. - Eur. J.* **2017**, *23*, 214−218.
(57) Atilgan, A.; Islamoglu, T.; Howarth, A. J.; Hupp, J. T.; Farha, O. K. Detoxification of a Sulfur Mustard Simulant Using a BODIPY-Functionalized Zirconium-Based Metal−Organic Framework. *ACS Appl. Mater. Interfaces* **2017**, *9*, 24555−24560.
(58) Abelard, J.; Wilmsmeyer, A. R.; Edwards, A. C.; Gordon, W. O.; Durke, E. M.; Karwacki, C. J.; Troya, D.; Morris, J. R. Adsorption of 2-Chloroethyl Ethyl Sulfide on Silica: Binding Mechanism and Energy of a Bifunctional Hydrogen-Bond Acceptor at the Gas−Surface Interface. *J. Phys. Chem. C* **2015**, *119*, 365−372.
(59) Stout, S. C.; Larsen, S. C.; Grassian, V. H. Adsorption, Desorption and Thermal Oxidation of 2-CEES on Nanocrystalline Zeolites. *Microporous Mesoporous Mater.* **2007**, *100*, 77−86.
(60) Grissom, T. G.; Driscoll, D. M.; Troya, D.; Sapienza, N. S.; Usov, P. M.; Morris, A. J.; Morris, J. R. Molecular-Level Insight into CO_2 Adsorption on the Zirconium-Based Metal−Organic Framework, UiO-66: A Combined Spectroscopic and Computational Approach. *J. Phys. Chem. C* **2019**, *123*, 13731−13738.
(61) Driscoll, D. M.; Troya, D.; Usov, P. M.; Maynes, A. J.; Morris, A. J.; Morris, J. R. Characterization of Undercoordinated Zr Defect Sites in UiO-66 with Vibrational Spectroscopy of Adsorbed CO. *J. Phys. Chem. C* **2018**, *122*, 14582−14589.
(62) Driscoll, D. M.; Troya, D.; Usov, P. M.; Maynes, A. J.; Morris, A. J.; Morris, J. R. Geometry and Energetics of CO Adsorption on Hydroxylated UiO-66. *Phys. Chem. Chem. Phys.* **2019**, *21*, 5078−5085.
(63) Hadjiivanov, K. I.; Vayssilov, G. N. Characterization of Oxide Surfaces and Zeolites by Carbon Monoxide as an IR Probe Molecule. *Adv. Catal.* **2002**, *47*, 307−511.
(64) Plonka, A. M.; Grissom, T. G.; Musaev, D. G.; Balboa, A.; Gordon, W. O.; Collins-Wildman, D. L.; Ghose, S. K.; Tian, Y.; Ebrahim, A. M.; Mitchell, M. B.; Hill, C. L.; Morris, J. R.; Frenkel, A. I. Effect of Carbon Dioxide on the Degradation of Chemical Warfare Agent Simulant in the Presence of Zr Metal Organic Framework MOF-808. *Chem. Mater.* **2019**, *31*, 9904−9914.
(65) Lv, H.; Geletii, Y. V.; Zhao, C.; Vickers, J. W.; Zhu, G.; Luo, Z.; Song, J.; Lian, T.; Musaev, D. G.; Hill, C. L. Polyoxometalate Water Oxidation Catalysts and the Production of Green Fuel. *Chem. Soc. Rev.* **2012**, *41*, 7572−7589.
(66) Kaledin, A. L.; Driscoll, D. M.; Troya, D.; Collins-Wildman, D. L.; Hill, C. L.; Morris, J. R.; Musaev, D. G. Impact of Ambient Gases on the Mechanism of $[Cs_8Nb_6O_{19}]$-Promoted Nerve-Agent Decomposition. *Chem. Sci.* **2018**, *9*, 2147−2158.
(67) Kaledin, A. L.; Troya, D.; Karwacki, C. J.; Balboa, A.; Gordon, W. O.; Morris, J. R.; Mitchell, M. B.; Frenkel, A. I.; Hill, C. L.; Musaev, D. G. Key Mechanistic Details of Paraoxon Decomposition by Polyoxometalates: Critical Role of Para-Nitro Substitution. *Chem. Phys.* **2019**, *518*, 30−37.
(68) Chapleski, R. C.; Musaev, D. G.; Hill, C. L.; Troya, D. Reaction Mechanism of Nerve-Agent Hydrolysis with the $Cs_8Nb_6O_{19}$ Lindqvist Hexaniobate Catalyst. *J. Phys. Chem. C* **2016**, *120*, 16822−16830.
(69) Kinnan, M. K.; Creasy, W. R.; Fullmer, L. B.; Schreuder-Gibson, H. L.; Nyman, M. Nerve Agent Degradation with Polyoxoniobates. *Eur. J. Inorg. Chem.* **2014**, *2014*, 2361−2367.
(70) Collins-Wildman, D. L.; Kim, M.; Sullivan, K. P.; Plonka, A. M.; Frenkel, A. I.; Musaev, D. G.; Hill, C. L. Buffer-Induced Acceleration and Inhibition in Polyoxometalate-Catalyzed Organophosphorus Ester Hydrolysis. *ACS Catal.* **2018**, *8*, 7068−7076.
(71) Balow, R. B.; Lundin, J. G.; Daniels, G. C.; Gordon, W. O.; McEntee, M.; Peterson, G. W.; Wynne, J. H.; Pehrsson, P. E. Environmental Effects on Zirconium Hydroxide Nanoparticles and Chemical Warfare Agent Decomposition: Implications of Atmospheric Water and Carbon Dioxide. *ACS Appl. Mater. Interfaces* **2017**, *9*, 39747−39757.
(72) Clausen, B. S.; Gråbæk, L.; Steffensen, G.; Hansen, P. L.; Topsøe, H. A Combined QEXAFS/XRD Method for On-line, In Situ Studies of Catalysts: Examples of Dynamic Measurements of Cu-based Methanol Catalysts. *Catal. Lett.* **1993**, *20*, 23−36.
(73) Tinnemans, S. J.; Mesu, J. G.; Kervinen, K.; Visser, T.; Nijhuis, T. A.; Beale, A. M.; Keller, D. E.; van der Eerden, A. M. J.; Weckhuysen, B. M. Combining Operando Techniques in One Spectroscopic-Reaction Cell: New Opportunities for Elucidating the Active Site and Related Reaction Mechanism in Catalysis. *Catal. Today* **2006**, *113*, 3−15.
(74) Patlolla, A.; Carino, E. V.; Ehrlich, S. N.; Stavitski, E.; Frenkel, A. I. Application of Operando XAS, XRD, and Raman Spectroscopy for Phase Speciation in Water Gas Shift Reaction Catalysts. *ACS Catal.* **2012**, *2*, 2216−2223.

https://dx.doi.org/10.1021/acsami.9b20833
ACS Appl. Mater. Interfaces 2020, 12, 14641−14661

(75) Frenkel, A. I.; Rodriguez, J. A.; Chen, J. G. Synchrotron Techniques for In Situ Catalytic Studies: Capabilities, Challenges, and Opportunities. *ACS Catal.* **2012**, *2*, 2269−2280.
(76) Liu, D.; Li, Y.; Kottwitz, M.; Yan, B.; Yao, S.; Gamalski, A.; Grolimund, D.; Safonova, O. V.; Nachtegaal, M.; Chen, J. G.; Stach, E. A.; Nuzzo, R. G.; Frenkel, A. I. Identifying Dynamic Structural Changes of Active Sites in Pt−Ni Bimetallic Catalysts Using Multimodal Approaches. *ACS Catal.* **2018**, *8*, 4120−4131.
(77) Zhao, S.; Li, Y.; Liu, D.; Liu, J.; Liu, Y.-M.; Zakharov, D. N.; Wu, Q.; Orlov, A.; Gewirth, A. A.; Stach, E. A.; Nuzzo, R. G.; Frenkel, A. I. Multimodal Study of the Speciations and Activities of Supported Pd Catalysts During the Hydrogenation of Ethylene. *J. Phys. Chem. C* **2017**, *121*, 18962−18972.
(78) Li, Y.; Zakharov, D.; Zhao, S.; Tappero, R.; Jung, U.; Elsen, A.; Baumann, P.; Nuzzo, R. G.; Stach, E. A.; Frenkel, A. I. Complex Structural Dynamics of Nanocatalysts Revealed in Operando Conditions by Correlated Imaging and Spectroscopy Probes. *Nat. Commun.* **2015**, *6*, 7583.
(79) Weckhuysen, B. M. Snapshots of a Working Catalyst: Possibilities and Limitations of In Situ Spectroscopy in the Field of Heterogeneous Catalysis. *Chem. Commun.* **2002**, 97−110.
(80) Grunwaldt, J. D.; Caravati, M.; Hannemann, S.; Baiker, A. X-Ray Absorption Spectroscopy Under Reaction Conditions: Suitability of Different Reaction Cells for Combined Catalyst Characterization and Time-Resolved Studies. *Phys. Chem. Chem. Phys.* **2004**, *6*, 3037−3047.
(81) Ebrahim, A. M.; Plonka, A. M.; Tian, Y.; Senanayake, S. D.; Gordon, W. O.; Balboa, A.; Wang, H.; Collins-Wildman, D. L.; Hill, C. L.; Musaev, D. G.; Morris, J. R.; Troya, D.; Frenkel, A. I. Multimodal Characterization of Materials and Decontamination Processes for Chemical Warfare Protection. *ACS Appl. Mater. Interfaces* **2019**, DOI: 10.1021/acsami.9b19494.

https://dx.doi.org/10.1021/acsami.9b20833
ACS Appl. Mater. Interfaces 2020, 12, 14641−14661